An autoregulation loop in *fust-1* for circular RNA regulation in *Caenorhabditis elegans*

Dong Cao

Information Processing Biology Unit, Okinawa Institute of Science and Technology Graduate University, 1919-1 Tancha, Onna, Kunigami, Okinawa, Japan, 904-0495

Corresponding author:

Dong Cao (dong.cao@oist.jp)

Running title: Autoregulation of *fust-1* for circRNA regulation

Keywords

circular RNA, FUS, RNA-binding protein, autoregulation, back splicing, alternative splicing

Abstract

Many circular RNAs (circRNAs) are differentially expressed in different tissues or cell types, suggestive of specific factors that regulate their biogenesis. Here, taking advantage of available mutation strains of RNA binding proteins (RBPs) in *Caenorhabditis elegans*, I performed a screening of circRNA regulation in thirteen conserved RBPs. Among them, loss of FUST-1, the homolog of FUS (Fused in Sarcoma), caused downregulation of multiple circRNAs. By rescue experiments, I confirmed FUST-1 as a circRNA regulator. Through RNA-seq using circRNA enriched samples, circRNAs targets regulated by FUST-1 were identified globally, with hundreds of them significantly altered. Further, I showed that FUST-1 regulates circRNA formation with only small to little effect on the cognate linear mRNAs. When recognizing circRNA pre-mRNAs, FUST-1 can affect both exon-skipping and circRNA in the same genes. Moreover, I identified an autoregulation loop in *fust-1*, where FUST-1, isoform a (FUST-1A) promotes the skipping of exon 5 of its own pre-mRNA, which produces FUST-1, isoform b (FUST-1B) with different N-terminal sequences. FUST-1A is the functional isoform in circRNA regulation. Although FUST-1B has the same functional domains as FUST-1A, it cannot regulate either exon-skipping or circRNA formation. This study provided an *in vivo* investigation of circRNA regulation, which will be helpful to understand the mechanisms that govern circRNA formation.

Introduction

Although treated as byproducts of splicing in early years (Cocquerelle et al. 1993; Nigro et al. 1991), circRNAs have shown diverse functions in different biological or physiological environments, including interactions with DNAs (transcription regulation (Li et al. 2015), R-loop structure formation (Conn et al. 2017)), RNAs (miRNA sponge (Hansen et al. 2013; Memczak et al. 2013)), and proteins (Du et al. 2020; Okholm et al. 2020; Xia et al. 2018; Zhu et al. 2019). Rather than splicing errors, the circRNA production process is well-regulated, in which both intronic sequences (*cis* elements) and RBPs (*cis/trans* elements) are involved (Chen 2020). Reverse complementary matches (RCMs, *cis* elements) in introns that flank exon(s) to be circularized promote circRNA formation, presumably by bringing splice sites for back-splicing together. RBPs (*cis*/*trans* elements) can regulate back-splicing positively or negatively. Muscleblind in *Drosophila* promotes the production of the circRNA from the second exon of its own pre-mRNA by binding to the flanking introns (Ashwal-Fluss et al. 2014). The splicing factor Quaking promotes circRNA biogenesis during epithelial to mesenchymal transition (Conn et al. 2015). Immune factors NF90/NF110 promote circRNA formation by associating with intronic RNA pairs in circRNA-flanking introns (Li et al. 2017). RBM20 in mice promotes the production of multiple circRNAs from the gene Tintin (Khan et al. 2016). ADAR1 (Ivanov et al. 2015; Rybak-Wolf et al. 2015) and DHX9 (Aktas et al. 2017) negatively regulate circRNAs by disturbing the base pairing of RCMs. Multiple heterogeneous nuclear ribonucleoproteins (hnRNPs) and serine–arginine (SR) proteins function in a combinatorial manner to regulate circRNAs in cultured *Drosophila* cells (Kramer et al. 2015). HNRNPL regulates circRNA levels in LNCaP cells by binding to circRNA-flanking introns (Fei et al. 2017). A recent paper shows that RBP FUS affects circRNA expression in stem cell-derived motor neurons in mice (Errichelli et al. 2017). All these findings were from *in vitro* cultured cells of different organisms. *C. elegans* provides a suitable animal model for *in vivo* study of circRNA regulation, given the conservation of RBPs and availability of diverse mutant strains.

FUS plays diverse roles in DNA repair and RNA splicing (Sama et al. 2014). Particularly, the mutation of FUS has been linked to the neurodegenerative disease ALS (Kwiatkowski et al. 2009; Vance et al. 2009). *C. elegans* has been used to model ALS by knocking in wild-type or mutated human FUS (Markert et al. 2019; Murakami et al. 2015; Murakami et al. 2012; Vaccaro et al.

2012a; Vaccaro et al. 2012b; Veriepe et al. 2015). As the homolog of FUS in *C. elegans*, FUST-1 is involved in lifespan and neuronal integrity regulation (Therrien et al. 2016) and miRNA-mediated gene silencing (Zhang et al. 2018).

Autoregulation feedback has been found in many RBPs, which is beneficial for them to maintain proper protein levels (Buratti and Baralle 2011; Muller-McNicoll et al. 2019). The mechanisms include autoregulation of alternative splicing (AS) of their own pre-mRNA, which either produces unproductive transcripts with premature termination codons that are subjected to nonsense-mediated decay (NMD) pathway (McGlincy et al. 2010; Rossbach et al. 2009; Sureau et al. 2001; Wollerton et al. 2004) or produces another protein isoform with disturbed functional domains (Damianov and Black 2010). Here, I identified an autoregulation pathway in the production of the two isoforms of FUST-1 in *C. elegans*.

Here, using available RBP mutation strains in *C. elegans*, I performed a screening of 13 conserved RBPs in their roles in circRNA regulation. FUST-1 stood out in the screening, showing promotional effects on the production of multiple circRNAs. I further checked FUST-1's role in circRNA regulation globally by RNA-seq with circRNA-enriched samples and identified many circRNAs regulated by FUST-1. FUST-1 recognizes pre-mRNAs of circRNA genes and can regulate both exon-skipping and circRNA production in the same genes. Moreover, I characterized an autoregulation loop in the production of the two isoforms of FUST-1, in which FUST-1A promotes the skipping of exon 5 of *fust-1* pre-mRNA, which produces FUST-1B. Interestingly, although FUST-1B has the same functional domains as FUST-1A, it cannot regulate exon-skipping or circRNA formation.

Materials and methods

Worm maintenance

C. elegans Bristol N2 strain was used as the wild type. Worms were maintained using standard conditions on Nematode Growth Media (NGM) agar plates with *Escherichia coli* strain OP50 (Brenner 1974) at 20°C or 25^{o}C. New transgenic worms were generated by microinjection with ~40 ng/μl plasmid. The strains used in this study are listed in TableS1.

Plasmid preparation

fust-1p::fust-1::mRFP: fust-1 genomic fragment containing sequences from 2181bp upstream ATG to just before stop codon was cloned into the Sma I site of pHK-mRFP vector in frame with mRFP by In-Fusion HD Cloning Kit (Takara). This plasmid was further used to generate the backbone structure containing *fust-1* promoter and mRFP, to which cDNAs of FUST-1 isoforms (isoform a, isoform b, and ΔN) were inserted by In-Fusion (Takara). The mRFP fused FUST-1 cDNA plasmids were used to generate cDNA-only plasmids for splicing reporter rescue by removing the mRFP sequences using In-Fusion (Takara). Splicing reporter of *fust-1* exon 5 was prepared by cloning exon 4 to exon 6 into the plasmids provided by Dr. Adam Norris.

Worm synchronization

Worm synchronization was performed by bleaching for large-scale worm preparation (RNA extraction). For small-scale worm preparation (locomotion assay), worms were synchronized by egg-laying. Briefly, 10 - 15 gravid adult worms were placed onto a seeded NGM plate for four hours, and worms were removed after egg-laying. The eggs were then cultured to the desired stage.

Worm sorting

L1 worms with extrachromosomal fluorescent proteins were obtained by bleaching and hatching overnight at room temperature. Then fluorescence-positive worms were sorted using BioSorter Large Particle Flow Cytometer (Union Biometrica).

DAPI staining

DAPI (4',6-diamidino-2-phenylindole) was used for DNA staining. Worms were fixed using 95% ethonal and then washed with PBS (137 mM NaCl, 2.7 mM KCl, 8 mM Na_2HPO_4, and 2 mM KH_2PO_4, pH 7.4). DAPI is added to a final concentration of 100 ng/ml and incubated at dark for ~ 20 min. Worms were washed with PBS twice and mounted on an agar pad for visualization using a confocal microscope.

Mutagenesis by CRISPR-Cas9

Mutation by CRISPR-Cas9 was performed as described previously (Cao 2021). For FLAG-tag insertion, single-stranded oligo DNAs (ssODNs) were used as repair fragments. For *fust-1::mRFP* and *fust-1a::mRFP* strain preparation, dsDNA repair fragments were amplified from the corresponding plasmids using primers containing recombinant sequences. Guide RNA sequences, recombinant ssODNs, validation primers, and primers for recombinant fragment amplification are listed in Table S3.

Co-immunoprecipitation (Co-IP)

~20,000 L1 FLAG::FUST-1 worms were seeded on a nutrition enriched plate with NA22 *E. coli* (NEP-NA22). After 4-day culture at 20^{o}C, all bacteria were consumed, and most of the progenies were at the L1 stage. Adult worms were removed by filtering through a 30 μm mesh. Three NEP-NA22 plates, which gave ~ 1 million L1 worms, were used for one replicate experiment. Worms were washed with 1 × 10 ml M9 buffer, 2 × 10 ml cold Buffer B70 (50 mM HEPES-KOH (pH 7.4), 70 mM potassium acetate (KAc), 1 mM sodium fluoride (NaF), 20 mM β-glycerophosphate, 5 mM magnesium acetate (MgOAc), 0.1% Triton X-100, 10% glycerol). Worms were then re-suspended in 0.4 ml Buffer B70 supplemented with 2 × cOmplete Proteinase inhibitor cocktail (Roche) and dripped into liquid N_2 with 1 ml pipette tips to form small pearls. Worm pearls were stored at -80^{o}C. Worm pearls were ground into fine powder in a mortar containing liquid N_2, which was suspended into 1 ml cold Buffer B70 supplemented with 2 × cOmplete Proteinase inhibitor cocktail (Roche) and 5 μl Murine RNase Inhibitor (NEB). Worm lysate was cleared by centrifugation at 20,000 × g for 20 min at 4^{o}C. 50 μl worm lysate was taken as input samples, in which 40 μl was used for RNA extraction and 10 μl for western blot. 50 μl Dynabeads Protein G (Invitrogen) was coupled with or without 5 μg Anti-FLAG M2 antibody (Sigma-Aldrich), which was then incubated with 400 μl lysate, rotating overnight at

4°C. The next day, the lysate-beads slurry was cleared magnetically, and the supernatant was taken for western blot. Keeping tubes on magnetic tray, the beads were washed 2 × 200 ul Buffer B70 gently. 50 µl 50 mM glycine, pH 2.8 was added to the washed beads to elute bound RBP complex. After mixing and incubating at RT for 3 min, the supernatant was transferred to another tube containing 5 µl 1 M Tris-HCl, pH 7.5 for pH neutralization. For the 55 µl elution, 44 µl was used for RNA extraction, 11 µl for western blot.

Western blot

Protein samples were resolved by SDS-PAGE (5% stacking gel and 12% resolving gel) and transferred to PVDF membrane by the standard protocol (25 V, 30 min) of Trans-Blot Turbo Transfer System (Bio-Rad). After blocking with 5% BSA-PBST (137 mM Sodium Chloride, 10 mM Phosphate, 2.7 mM Potassium Chloride, pH 7.4, 0.1% (v/v) Tween-20, and 5% (w/v) BSA) for 1 hour at room temperature, the membrane was incubated overnight with primary antibody (listed below) at 4°C. After 3 × 5 min washes in PBST, the membrane was incubated with HRP-conjugated secondary antibody at room temperature for 1 hour. The membrane was washed 3 × 5 min in PBST and then visualized by Amersham ECL Prime Western Blot Detection Reagent (GE Healthcare). Images were taken by Fluorescent Image Analyzer LAS-3000 (FujiFilm) using the chemiluminescence channel. Mouse ANTI-FLAG M2 antibody (F3165, Sigma-Aldrich): 1:2000; Amersham ECL Mouse IgG, HRP-linked whole Ab (from sheep):1:2000.

RNA extraction

RNA extraction was performed using Direct-zol RNA MicroPrep kit (ZYMO Research) with on-column DNase I (ZYMO Research) digestion according to the manufacturer's protocol. For RNA extraction from worms, worms were first flash-frozen in Trizol solution (Invitrogen) in liquid N_2 and then homogenized by vortexing with glass beads (φ 0.1 mm) in Beads Cell Disrupter MS-100 (TOMY).

circRNA enrichment by RPAD

RPAD was performed as the reported protocol (Panda et al. 2017). Briefly, 10 µg total RNA from L1 stage of wild-type (N2) strain or *fust-1(csb21)* strain was heated for 10 min at 65°C and then put on ice for 2 min. Then the denatured RNA was treated with RNase R in a 50 µl reaction containing 50 U RNase R (E049, abm), 100 U RNase Inhibitor, Murine (NEB), 1 × RNase R

buffer for 30 min at 37°C. RNase R-treated RNA was purified with RNA Clean and Concentrator-5 kit (ZYMO Research) and eluted with 20.5 μl H_2O following manufacturer's protocol. 20 μl of eluted RNA was denatured as before and then mixed with 1 × Poly(A) Polymerase Reaction Buffer, 40 U RNase Inhibitor, Murine (NEB), 10 U *E. coli* Poly(A) Polymerase (NEB), 1 mM ATP in a 40 μl reaction and incubated at 37°C for 30 min. 100 μl Oligo $d(T)_{25}$ Magnetic Beads (S1419S, NEB) was washed twice with 300 μl 2 × Binding buffer (200mM Tris-HCl, pH 7.5, 1 M LiCl, 1% Lithium Dodecyl Sulfate (LiDS), 2 mM EDTA, 10 mM DTT) and then re-suspended in 40 μl 2 × Binding buffer. The 40 μl polyadenylation mix was added to the equilibrated beads and the mixture was incubated at 75°C for 5 min followed by 20 min at 25°C with periodic mixing by gentle vortex. The supernatant was taken by put on the mixture on a magnetic rack for 2 min. Before purification with RNA Clean and Concentrator kit (ZYMO Research), 80 μl H_2O was added to dilute the salt content. RNA was eluted with 13 μl H_2O, and 11 μl was used for library preparation.

RNA Sequencing

Total RNA samples were from the L1 stage of N2 and *fust-1(csb21).* For RNA-seq with ribo-depletion only (ribo$^-$), 500 ng total RNA samples from 3 biological duplicates were used as inputs. rRNA depletion was performed using Ribo-Zero Plus rRNA Depletion kit (Illumina), and library preparation was conducted using NEBNext Ultra II Directional RNA Library Prep Kit for Illumina (New England BioLabs) according to manufacturer's protocols. For circRNA enriched samples, 10 μg total RNA was used for RPAD treatment, which was then subjected to rRNA depletion with Ribo-Zero Plus rRNA Depletion kit (Illumina) and library preparation with NEBNext Ultra II Directional RNA Library Prep Kit for Illumina (New England BioLabs). Sequencing was performed on NovaSeq 6000 (Illumina) to obtain 150 nt and 50 nt paired-end reads for ribo$^-$ samples and RPAD samples, respectively.

Real-time PCR

Real-time PCR reactions were performed using soAdvanced Universal SYBR Green Supermix (Bio-Rad) with cDNAs synthesized from iScript Advanced cDNA synthesis kit (Bio-Rad). 20 μl reaction mix with 2 μl cDNA (~1-10 ng) were monitored on StepOnePlus Thermal Cycler (Applied Biosystems) in "fast mode". Cycling conditions: 95 °C, 30', 40 or 45 cycles of 95 °C,

15’ and 60 °C, 30’with plate reading, and a final melt curve stage using default conditions. If not mentioned, all cDNAs used for RT-qPCR were from the L1 stage of indicated strains. If Ct values were not determined or higher than Ct values in no-template control (NTC) samples, they are treated as “n.d.” (not detected). Primers used for RT-qPCR are listed in Table S2.

Northern blot

Northern blot was performed using NorthernMax kit (ThermoFisher Scientific) as described previously (Cao 2021). Probes were labeled by α-32P-deoxycytidine 5'-triphosphate (PerkinElmer) using Random Primer DNA Labeling Kit Ver. 2 (Takara, #6045) according to manufacturer’s protocols. Here, total RNA samples (5 μg each) from L1 worms of N2 and *fust-1(csb21)* were used. Quantification of band intensities was performed using ImageQuant software (GE Healthcare). The average intensity of an area with no bands was used as background intensity. The average intensities of each band were subtracted by the background intensity before comparison (Figure S3B). Signals from *act-1* were used for normalization. Primers used for probe amplification are in Table S2.

circRNA prediction and RNA-seq data analysis

circRNA prediction from the RPAD dataset was performed by using three methods, CIRI2, DCC, and CIRCexplorer2, with the developers’ recommended parameters. Brifely, For DCC, raw reads were aligned to reference genome (WBcel235/ce11) using STAR (Dobin et al. 2013) (https://github.com/alexdobin/STAR) with the following options: --outSJfilterOverhangMin 15 15 15 15 –alignSJoverhangMin 15 –alignSJDBoverhangMin 15 --outFilterScoreMin 1 --outFilterMatchNmin 1 --outFilterMismatchNmax 2 --chimSegmentMin 15 --chimScoreMin 15 --chimScoreSeparation 10 --chimJunctionOverhangMin 15. Then the output files from STAR, chimeric.out.junction, were used for circRNA annotation with DCC (https://github.com/dieterich-lab/DCC). For CIRI2, RNA-seq reads were aligned to WBcel235/ce11 genome by BWA with the following scripts (using N2_1 as an example):

```
bwa mem -T 19 -t 64 /path/to/genome.fa N2_1_R1_001.fastq.gz N2_1_R2_001.fastq.gz > N2_1.sam
```

```
perl ./CIRI2.pl -I ./N2_1.sam -O N2_1_all -F /path/to/genome.fa -A /path/to/genes.gtf -T 12 -0
```

For CIRCexplorer2, RNA-seq reads were aligned using STAR with the following option: --chimSegmentMin 10. Then annotation was performed following the recommended conditions in the manual (https://circexplorer2.readthedocs.io/en/latest/). The overlapped circRNAs were further filtered with at least 15 BSJ reads determined by CIRI2. The filtered circRNAs were listed in Table S5. For differential expression (DE) analysis by DESeq2, read counts of mRNAs from the ribo$^-$ dataset and the BSJ read counts from the RPAD dataset annotated by CIRI2 were used as inputs for linear mRNA and circRNA, respectively. DE analysis results were in Table S6 and S7. The ggplot2 package (https://ggplot2.tidyverse.org/), and ggpubr (http://www.sthda.com/english/rpkgs/ggpubr) package were used to make the scatter plots.

Gene ontology enrichment analysis

Gene ontology enrichment analysis was performed using WormBase Enrichment Suite webserver (https://wormbase.org/tools/enrichment/tea/tea.cgi) (Angeles-Albores et al. 2018; Angeles-Albores et al. 2016).

Microscopy

Confocal images were obtained using a Zeiss LSM780 confocal microscope.Worms were immobilized using NaN_3 (50 mM in M9) and mounted on agar pads. For mCherry-to-GFP ratio quantification of splicing reporter of *fust-1* exon 5, all images were taken under the same setting parameters (Pinhole: 1.00 AU; Laser: 561 nm, 2.00%, 488 nm, 2.00%; Detection wavelength: GFP, 493-556 nm, mCherry, 588-694 nm; Gain: GFP, 625.0, mCherry, 790.0; Detector Digital Gain: 1.0 for all channels) to make sure that no saturation in both GFP and mCherry channels. Images were processed using ZEISS ZEN3.1 software. The average intensities in the GFP channel and the mCherry channel were used for quantification.

Locomotion Assay

Locomotion analysis of day 3 adult worms was performed as described previously (Kawamura and Maruyama 2019). Briefly, 15 synchronized day 3 adult worms were picked onto a blank NGM plate to get rid of food for ~1 min. The worms were then transferred to another empty NGM plate, and locomotion images were recorded for 1min with five frames per second with the lid on. Images were analyzed using ImageJ and wrMTrck plugin (Nussbaum-Krammer et al.

2015) (http://www.phage.dk/plugins/wrmtrck.html) to calculate the average speeds. More than 50 worms were recorded. Worms lost during recording were not included.

Prion-like domain prediction

PrLD prediction was performed using the web application of PLAAC (http://plaac.wi.mit.edu/) (Lancaster et al. 2014).

Results

1. RBP screening identifies FUST-1 as a circRNA regulator

Previous studies have shown that circRNAs are expressed in a tissue-specific and well-regulated manner (Chen and Schuman 2016; Gruner et al. 2016; Memczak et al. 2013; Rybak-Wolf et al. 2015; Westholm et al. 2014; You et al. 2015), suggesting the existence of specific factors that regulate circRNA production. Here, taking advantage of the available RBP mutants in *C. elegans*, I aimed to identify potential circRNA regulators *in vivo*.

In my previous study (Cao 2021), I obtained the neuronal circRNA profile at the L1 stage of *C. elegans*, in which circRNAs from the sorted neuron samples (the sort group) were compared with those in whole worm samples (the whole group). Several circRNAs that were either neuron-enriched or highly expressed in neurons were selected as targets (Figure S1A-B) (Cao 2021). The back-spliced junction (BSJ) sequences of the eight circRNAs and their resistance to RNase R digestion have been confirmed previously using the same divergent primers (Cao 2021) (Figure 1B and Table S2). Here, the full sequences of *circ-glr-2* were reconstituted by using two sets of divergent primers that cover the whole exons, confirming that only exons are retained (Figure S1C-D).

Thirteen RBPs that are conserved and have expressions in the neurons were chosen as potential regulators (Norris et al. 2017). Using mutant strains of these RBPs, a screening by RT-qPCR was performed to check the level changes of selected circRNAs in these mutant strains compared with wild-type N2 strain at the L1 stage (Figure 1A-B). As expected, levels of some circRNAs were altered in these mutant strains. Interestingly, most level changes of the selected circRNAs in these mutants were downregulations, suggestive of these RBPs' beneficial roles in circRNA production. Moreover, multiple neuron-enriched circRNAs (*circ-glr-2*, *circ-iglr-3*, *circ-arl-13*, *circ-cam-1*) were found to be downregulated in several strains (*asd-1(csb32)*, *tiar-3(csb35)*, *fox-1(csb39)*, *mec-8(csb22)*, *hrpf-1(csb26)*, and *fust-1(csb21)*) (Figure 1A), suggesting the regulation of these circRNAs by multiple RBPs. This is consistent with their roles in alternative splicing, where combinational regulation of one target by multiple RBPs is common in *C. elegans* (Tan and Fraser 2017). In line with this, no additive effect in circRNA regulation was found in *fust-1(csb21); hrpf-1(csb26)* double mutant strain compared with *fust-1(csb21)* single mutation

(Figure S2A), suggesting that the two RBPs may function as parts of a whole RNA-protein complex.

In these strains, *fust-1(csb21)* showed the most substantial downregulation of multiple circRNAs (Figure 1A). Hence it was chosen for further investigation. The downregulation of these circRNAs was also found in another *fust-1* mutant strain *fust-1*(*tm4439)* (Figure 1C-D), which is reported to be hypomorphic (Therrien et al. 2016). To further confirm the role of *fust-1* in circRNA regulation, a rescue strain (*fust-1(csb21); Ex[fust-1::mRFP]*) and an overexpression strain (*Ex[fust-1::mRFP]*) were made with extrachromosomal expression of *fust-1* genomic sequence, starting from *fust-1* promoter (2181 bp upstream ATG) to just before the stop codon of *fust-1*. Monomeric red fluorescent protein (mRFP) was fused to the C-terminal with a linker to check expression patterns. The expression of FUST-1 was mainly in the nuclei of neurons and intestinal cells (Figure 1E, Figure S2B-C). The mRFP-positive L1 worms from the rescue strain and the overexpression strain were sorted, and levels of the circRNAs were checked by RT-qPCR. As expected, the levels of downregulated circRNAs were restored in the rescue strain, confirming *fust-1*'s role in promoting circRNA production (Figure 1F). The *fust-1(csb21)* strain also showed another phenotype of lower average moving speed at day three adult stage when cultured at 25^{o}C, which was also recovered in the rescue strain (Figure S2D). Although multiple copies of *fust-1* existed in the extrachromosomal arrays of the rescue and the overexpression strain (Figure S2E), these strains did not show much further improvement in circRNA levels (except *circ-iglr-3*) or improvement in locomotion speed (Figure 1F and Figure S2D). This may be because of post-transcriptional regulation of *fust-1* or saturation of FUST-1 protein.

2. FUST-1 regulates circRNAs with small to little effect on the cognate linear mRNAs

Next, to clarify whether FUST-1 promotes circRNA production by transcription promotion or not, levels of circRNAs and their cognate linear mRNAs were compared between the N2 strain and *fust-1(csb21)* strain at the L1 stage. While levels of these circRNAs were downregulated, their linear mRNA levels were not affected by the loss of FUST-1 (Figure 2A-B), indicating that FUST-1's role in circRNA production is not through promoting transcription. In *zip-2*, northern blot detection using a probe (Figure 2C, probe 1) that detects both the full-length mRNA and the circular transcript gave two bands with their sizes being the theoretical lengths of *L-zip-2* and *circ-zip-2* (Figure 2D). To confirm that the lower bands are indeed *circ-zip-2*, another probe was used to detect *circ-zip-2* only (Figure 2C, probe 2). Although with some unspecific rRNA signals, this probe showed bands in the same positions as the lower bands using probe 1 (Figure S3A). Quantification of northern blot results of probe 1 showed that *circ-zip-2* was ~50% downregulated in *fust-1(csb21),* whereas *L-zip-2* was only slightly affected (Figure 2E and Figure S3B).

To check the regulation of circRNA by FUST-1 globally, RNA sequencing (RNA-seq) with ribosomal RNA depletion (ribo$^-$) was performed to compare differentially expressed circRNAs between *fust-1(csb21)* strain and wild-type N2 strain at the L1 stage. However, due to the low efficiency of *C elegans* rRNA depletion by commercial kits, the back-spliced junction (BSJ) reads that can be used for circRNA annotation and differential analysis were limited. Hence, RNA-seq using circRNA-enriched samples was performed, which was achieved by a published protocol using RNase R treatment followed by polyadenylation and poly(A)$^+$ RNA depletion (RPAD) (Panda et al. 2017) (Figure 2F). The RNA-seq with ribo-depletion only was used for mRNA comparison, and RNA-seq with RPAD was used for circRNA comparison. In order to increase circRNA annotation accuracy (Hansen 2018), three algorithms (DCC (Cheng et al. 2016), CIRI2 (Gao et al. 2018), and CIRCexplorer2 (Zhang et al. 2016)) were used, from which the overlapped circRNAs were further filtered with at least 15 BSJ reads in either the N2 group or the *fust-1(csb21)* group, which results in a dataset containing 4956 circRNAs derived from 2280 genes (Figure S3C and Table S5). As expected, the RPAD method effectively enriched circRNAs and increased the BSJ read numbers for circRNA annotation (Figure 2G and Figure S3D-E). TPM (transcripts per million reads) values of circRNAs and their cognate mRNAs were

compared between the two strains. With a cutoff of 1.5-fold change between the two strains, many circRNA levels were altered (Figure S3F). However, only limited numbers of circRNA genes were de-regulated (Figure 3G). Especially for circRNAs with high TPM values in N2 (top 400), circRNAs showed downregulation in *fust-1(csb21)* were much more than upregulated ones (208 vs. 25, Figure S3H).

Then, circRNA and mRNA differential expression (DE) analysis was performed using DESeq2 (Love et al. 2014) with fold-change shrinkage estimation by "ashr" method (Stephens 2017). For circRNAs, due to different efficiencies of circRNA enrichment in each gene, only the BSJ reads were used for DE analysis. With a cutoff of fold change > 1.5 and adjusted p value < 0.05, 270 mRNAs (95 upregulated, 175 downregulated) and 330 circRNAs (181 upregulated and 149 downregulated) were significantly altered in *fust-1(csb21)* compared with the N2 group (Table S6, S7). To check whether level changes in circRNA correlate with their cognate linear mRNAs, the fold changes of circRNA were plotted against those of their cognate mRNAs. The results showed little correlation (Figure 2H, Pearson's correlation coefficient $R = 0.038$, $p = 0.0076$), which were consistent with the finding that FUST-1 regulates circRNAs with small to little effect on the cognate linear mRNAs (Figure 2B).

Gene ontology enrichment analysis of differentially expressed mRNAs or circRNAs was performed (Table S8). Upregulated mRNAs and downregulated circRNAs did not show any significantly enriched terms. Downregulated mRNAs showed highly enriched terms in cuticle and collagen functions since many collagen genes were downregulated (Table S7, S8). As for upregulated circRNAs, terms related to neuronal functions are enriched, like neuron differentiation and neurogenesis (Table S8). Given this, I then asked whether FUST-1 has a preference in the regulation of neuronal circRNAs. In my previous study, I provided the first neuronal circRNA profiles at the L1 stage of *C. elegans* by comparing circRNAs in sorted neuron samples (the sort group) and whole worm samples (the whole group) (Cao 2021). The circRNAs identified in the RPAD dataset were compared with my previous dataset (the "sort & whole" dataset), which resulted in 910 overlapped circRNAs (Figure S3I). Fold changes of the 910 overlapped circRNAs between *fust-1(csb21)* and N2 were plotted against those between the sort group and the whole group, which showed no correlation (Figure 2I, Pearson's correlation

coefficient R = -0.0092, p = 0.78), suggesting that although FUST-1 can regulate many circRNAs from neuronal genes, it has no preference for neuronal circRNAs.

3. FUST-1 binds to pre-mRNAs of circRNA genes

FUS binds to flanking introns of circRNA genes in mouse neuroblastoma N2a cells (Errichelli et al. 2017). I next checked whether FUST-1 in *C. elegans* recognizes pre-mRNAs of circRNA genes to regulate circRNA formation. By CRISPR-Cas9 technology (Dokshin et al. 2018), a FLAG tag was inserted to the N terminal, just after the start codon, or to the C-terminal, just before the stop codon, respectively (Figure 3A and Figure S4A). The effect of FLAG-tag insertion on FUST-1's role in circRNA regulation was evaluated. While N-terminal FLAG insertion showed slight increases in circRNA levels, C-terminal FLAG tag fusion affected FUST-1's function in circRNA regulation in multiple circRNAs (Figure S4B-C). Hence N-terminal FLAG fused FUST-1 strain was used for the co-immunoprecipitation (Co-IP) experiment. Dynabeads Protein G conjugated with anti-FLAG antibody (+Ab) were used for Co-IP. Beads only (-Ab) were used as the negative control. As expected, the anti-FLAG antibody successfully enriched FLAG::FUST-1 after Co-IP (Figure 3B and Figure S4D). Then the levels of pre-mRNAs of circRNA genes were quantified by RT-qPCR. Threshold cycle (Ct) values were used for comparison. Lower Ct values indicate higher levels. Here, *18S rRNA* and *26S rRNA* were used as control RNA molecules, since I found that pre-RNAs of two house-keeping genes (*pmp-3* and *cdc-42*) were also enriched after Co-IP (Figure S4E-F), which may be because of FUST-1's interaction with U1 snRNA (Figure S4G) or RNA polymerase II, as reported in FUS in human cells (Jutzi et al. 2020; Schwartz et al. 2012). While both *18S rRNA* and *26S rRNA* were depleted after Co-IP, the pre-mRNAs of circRNA genes were enriched compared with input samples (Figure 3C). Moreover, these pre-mRNAs showed significantly lower Ct values than those of control groups without using of antibody (Figure 3C), suggesting that FUST-1 binds to pre-mRNAs of the circRNAs genes to regulate circRNA formation.

4. FUST-1 regulates both exon-skipping and back-splicing

circRNA formation has been correlated to exon-skipping (Kelly et al. 2015). In my previous study, transcripts that skip the exons to be circularized were identified in several circRNA genes (Cao 2021) (Figure 4A). As the homolog of FUST-1 in humans and mice, FUS is involved in the regulation of alternative splicing of many genes by binding to their pre-mRNAs (Dichmann and Harland 2012; Ishigaki et al. 2012; Rogelj et al. 2012). Since FUST-1 binds to the pre-mRNAs of these circRNA genes, I then checked whether FUST-1 could also regulate exon-skipping or not. In the ribo$^-$ dataset, reads aligned to the skipped junction of *zip-2* were much less abundant in the *fust-1(csb21)* strain (27.0 reads on average) than those in the wild-type N2 strain (71.3 reads on average) (Figure 4B). The RT-qPCR quantification results also showed that both the circRNA and the skipped transcript in *zip-2* were downregulated in the absence of FUST-1 (Figure 4C). In *arl-13*, while the circRNA got downregulated in *fust-1(csb21)*, the skipped transcript was weakly upregulated (Figure 4D). These results suggest that FUST-1 may function differently in different genetic environments.

5. An autoregulation loop in *fust-1*

FUST-1 protein has two isoforms: FUST-1A is from the full-length transcript, and FUST-1B is from the transcript with skipped exon 5 (Figure 5A). Moreover, FUST-1B is translated using a downstream AUG and a different reading frame (+1) compared with FUST-1A. The reading frame in FUST-1B becomes the same as in FUST-1A after the skipping of exon 5 (38 nt in length). This results in a shorter FUST-1B (390 aa) with different N-terminal sequences, but the RNA recognition motif (RRM), zinc-finger (ZnF) domain, and the nuclear localization signal (NLS) domain are the same as FUST-1A (448 aa) (Figure 5A). To check how these two isoforms are expressed, two plasmids with different colors and a nonsense mutation in the reading frame of either isoform a (*fust-1a-mut::mRFP*) or isoform b (*fust-1b-mut::GFP*) were constructed so that only the other isoform can be expressed (Figure 5A and Figure S5A). Co-injection of the two plasmids in wild-type N2 strain showed that the two isoforms of FUST-1 were co-expressed in the nuclei of the same cells: neurons and intestinal cells (Figure 5B and Figure S5B). Interestingly, in early eggs, FUST-1A was expressed earlier than FUST-1B (Figure 5C). Furthermore, *fust1a-mut::GFP* plasmid expressed faintly in *fust-1(csb21)* strain and co-injection with *fust1b-mut::mRFP* can increase the GFP intensity (data not shown). These results gave a hint that FUST-1A may promote the production of FUST-1B.

To prove this hypothesis, I constructed a dual-color splicing reporter (Norris et al. 2014; Thompson et al. 2019) of the skipping of exon 5 in *fust-1* with a neuronal promoter, in which no skipping gives GFP expression while skipping of exon 5 results in mCherry expression (Figure S5C). As expected, two colors were co-expressed in almost all the neurons in the wild-type strain (Figure 5D), suggesting that exon-skipping of exon 5 is happening in all the neurons. However, when the reporter plasmid was crossed into two *fust-1* mutation strains, *fust-1(csb21)* and *fust-1(tm4439)* (Figure 1C), the expression of mCherry was dramatically reduced (Figure 5D and Figure S5D), indicating FUST-1 was involved in the exon-skipping of its own pre-mRNA. Since *fust-1(csb21)* strain has pharyngeal GFP expression (Norris et al. 2017) (Figure 1C and Figure 5D), neurons in the ventral nerve cord around the neck were used to quantify the mCherry-to-GFP intensity ratios (Figure 5D and Figure S5D). The mCherry-to-GFP ratios were significantly reduced in both two *fust-1* mutants, and they did not change in the *mec-8(csb22)* strain (Figure

5E and Figure S5D), suggesting a specific requirement of FUST-1 for the skipping of exon 5 for *fust-1* pre-mRNA.

Next, to prove that FUST-1A promotes the skipping of exon 5 of *fust-1* pre-mRNA, I tried the rescue of mCherry expression of the splicing reporter in *fust-1(csb21)* by co-injection of the reporter plasmid with FUST-1A cDNA or FUST-1B cDNA, driven by the *fust-1* original promoter (2181 bp upstream the ATG of FUST-1A). One more construct with truncated N-terminal (FUST-1-ΔN) was also used (Figure S6A). Tail-expressing plasmid *lin-44p::mRFP* was used as an injection marker. As expected, FUST-1A cDNA restored the mCherry expression of the splicing reporter, while FUST-1B cDNA did not (Figure 5F, Figure S6B-C), which confirms that FUST-1A promotes the skipping of exon 5 to produce FUST-1B. Consistent with this, *fust-1* pre-mRNA, detected by primers in intron 4 of *fust-1*, was significantly enriched after Co-IP with FLAG::FUST-1, which only tagged FUST-1A (Figure 5G). To my surprise, the FUST-1-ΔN construct also rescued the mCherry expression, just as efficient as FUST-1A (Figure 5F and Figure S6D). Since the three isoforms have identical functional domains (RRM, ZnF, and NLS) with different N-terminal sequences, these results suggest that the N-terminal sequences in FUST-1A may not be so crucial for its function, and the N-terminal in FUST-1B may prevent its domains from functioning normally.

Taken together, I characterized an autoregulation loop in *fust-1*, in which FUST-1A promotes the skipping of exon 5 of *fust-1* pre-mRNA, resulting in the production of FUST-1B.

6. FUST-1A is the functional isoform in circRNA regulation

Next, to check which isoform of FUST-1 is functional in circRNA regulation, I tried to rescue the downregulated circRNAs in *fust-1(csb21)* with extrachromosomal expression of FUST-1 isoform cDNA with C-terminal mRFP fusion, in which either FUST-1A, FUST-1B, or FUST-1-ΔN is expressed (Figure S7A). The mRFP-positive L1 worms were sorted, from which total RNA was extracted, and then circRNA levels were quantified by RT-qPCR. Same with their roles in exon-skipping, FUST-1A successfully rescued the downregulated circRNAs, whereas FUST-1B did not improve the downregulated circRNA levels at all, indicating that FUST-1A is the functional protein in circRNA regulation (Figure 6A). Although not as efficient as FUST-1A, FUST-1- ΔN fully rescued the downregulated *circ-zip-2* and *circ-iglr-3* and partially restored *circ-arl-13* level (Figure 6A).

In an effort to generate strains with endogenous C-terminal mRFP tagging of FUST-1 isoforms, I achieved C-terminal mRFP insertion in *fust-1* (*fust-1::mRFP*) by CRISPR-Cas9 (Table S3). Another obtained strain, in which intron 3 to intron 6 of *fust-1* were removed, cannot use the autoregulation pathway, resulting in the expression of only FUST-1A (*fust-1a::mRFP*) (Figure S7B). I failed to obtain a strain that can only express mRFP tagged FUST-1B. Consistent with the extrachromosomal expression pattern of FUST-1 (Figure 1E and Figure S2B-C), endogenously mRFP-tagged FUST-1 was mainly expressed in the nucleus of neurons and intestinal cells (Figure S7C). Moreover, FUST-1 was also found in the nuclei in gonads (Figure S7D), which was not observed in extrachromosomal expression, probably due to silencing of the multicopy transgenes in the germline (Merritt and Seydoux 2010). Levels of circRNAs were compared between *fust-1::mRFP* and *fust-1a::mRFP* to check whether loss of the autoregulation loop affects circRNA levels. Out of the five checked circRNA, the levels of four circRNAs were altered in the strain where only FUST-1A can be expressed (Figure 6B, *fust-1a::mRFP* vs. *fust-1::mRFP*), suggesting the autoregulation loop is important for FUST-1's role in circRNA regulation. For unknown reasons, some circRNA levels were increased after mRFP tagging (Figure 6B, N2 vs. *fust-1::mRFP*).

The FUST-1A-specific N-terminus has high ratios of glycines (53/164, 32.3%) and glutamines (22/164, 13.4%), a feature of low-complexity regions in proteins, such as prion-like domains (PrLDs) (King et al. 2012). Based on a PrLD prediction method, PLAAC (Lancaster et al. 2014),

the FUST-1A N-terminal sequences showed a high probability of being a PrLD (Figure 6C). However, for the N-terminus of FUST-1B, it was very unlikely to be a PrLD (Figure 6D). The frameshift in FUST-1B dramatically changes its amino acid contents, resulting in more valines (18/106, 17.0%) and glutamic acid residues (18/106, 17.0%), which are very few in isoform a-specific N-terminal: 0/164 and 2/164, respectively. The drastically different sequences between the N-termini of FUST-1A and FUST-1B may render them different folding conformations, dictating their distinct roles in regulating exon-skipping and back-splicing.

Discussion

Using identified circRNAs in the neurons as targets (Cao 2021), I performed a small-scale screening of thirteen conserved RBP genes in their roles in circRNA regulation. Most of these RBPs showed promotional roles in circRNA production, suggesting that the involvement of RBPs in back-splicing may be common in *C. elegans*. I further showed that FUST-1, the homolog gene of FUS in *C. elegans*, regulates circRNA formation with mild to little effect on their cognate mRNAs (Figure 2). Although I used circRNAs either enriched in neurons or highly expressed in neurons as targets to identify FUST-1, FUST-1 did not show preference in the regulation of neuronal circRNAs (Figure 2I). Since FUST-1 is also expressed in intestine and germline cells, FUST-1 may regulate circRNAs in those cells.

Previous CLIP-seq data on FUS suggest that rather than recognizing specific sequences, FUS tends to bind to stem-loop secondary structures (Hoell et al. 2011; Ishigaki et al. 2012; Rogelj et al. 2012; Zhou et al. 2013). Further, FUS's binding with RNA Polymerase II and U1 snRNA associates transcription with splicing (Jutzi et al. 2020; Schwartz et al. 2012; Yu and Reed 2015). In *C. elegans*, FUST-1 also can associate with U1 snRNA (Figure S4G). Here, I found that as well as the pre-mRNAs of circRNA genes regulated by FUST-1, some other pre-mRNAs were also enriched by Co-IP with FLAG::FUST-1. The results here cannot distinguish whether these enrichments were due to direct binding of FUST-1 or through FUST-1's interaction with U1 snRNA, which recognizes 5' splice sites of pre-mRNAs. Nevertheless, FUST-1 is involved in the back-splicing process of these circRNA genes. Moreover, FUST-1 can regulate both back-splicing and exon-skipping in *zip-2* and *arl-13*. In my previous work, I discovered that RCMs in circRNA-flanking introns of *zip-2* simultaneously promote both exon-skipping and back-splicing (Cao 2021). It is possible that the interaction sites of *zip-2* pre-mRNA with FUST-1 are in the flanking pair of introns, so that both processes can be regulated together.

Endogenous N-terminal FLAG tagging and C-terminal fusion of mRFP with a linker resulted in increased circRNA formation in several circRNA genes (Figure S4B and Figure 6B). However, direct FLAG tagging without a linker at the C-terminus showed reduced levels of circRNAs (Figure S4C). These results suggest that the terminal folding of FUST-1 can be affected by different tags, and a linker sequence may be necessary for C-terminal tagging.

Self-regulation has been reported in FUS, where FUS promotes skipping of exon 7 of its pre-mRNA, which results in NMD (Zhou et al. 2013). Unlike the previous example, FUST-1A-promoted exon skipping of *fust-1* pre-mRNA produces FUST-1B that contains exactly the same functional domains, but with different N-terminal sequences. While FUST-1A is capable of promoting exon-skipping and circRNA regulation, FUST-1B is not functional in either of the two aspects (Figure 5F, Figure 6A, and Figure 7). This is quite reasonable. Since if FUST-1B could promote the autoregulation, it would form positive feedback, which results in the accumulation of FUST-1B. This autoregulation loop serves as a pathway to regulate the level functional FUST-1 isoform: once FUST-1A's level is high, it promotes the production of non-functional FUST-1B, which consumes the pre-mRNA of *fust-1*, resulting in reduced production of FUST-1A (Figure 7).

Regarding the different functions of the two isoforms, I first hypothesized that N-terminal sequences in FUST-1A might be important for its function. However, the FUST-1-ΔN construct, which has no N-terminal sequences, appeared functional in both exon-skipping promotion and circRNA regulation, although not as efficient as FUST-1A. These results suggest that N-terminus in FUST-1B may interfere with the functional domain(s), possibly RRM, so that FUST-1B cannot bind to the target mRNAs recognized by FUST-1A. Indeed, PrLD prediction of the N-termini of the two isoforms showed that FUST-1A N-terminus has a high probability to be a PrLD, while the N-terminus of FUST-1B is very unlikely to fold like a PrLD (Figure 6C-D). Further *in vitro* RNA binding experiments or structural analysis may be worth trying to investigate the detailed mechanisms that dictate different function potentials in the two FUST-1 isoforms.

Data availability

Raw FASTQ files from the RNA-seq data were deposited at the NCBI Sequence Read Archive (BioProject: PRJNA669975(ribo$^-$) and PRJNA742881(RPAD), Table S4). All strains, plasmids, and other materials are available upon request.

Acknowledgment

I thank Dr. Adam Norris from the Department of Biological Sciences at Southern Methodist University for providing the RBP strains and the dual-color splicing reporter plasmids. I thank Dr. Alex Parker from the Department of neuroscience, Université de Montréal for providing a strain from which the *fust-1(tm4439)* strain was outcrossed. I thank DNA Sequencing Section of OIST for its help on library preparation and RNA sequencing of N2 and *fust-1(csb21)* samples. I thank the Information Processing Biology Unit (Maruyama Unit) members for their discussion and feedback. I am grateful for the help and support provided by the Scientific Computing and Data Analysis section of the Research Support Division at OIST.

Author Contributions

D.C. designed and conducted all the experiments, performed all the analysis, and wrote the paper.

Declaration of Interests

The author declares no competing interests.

Funding

I thank Okinawa Institute of Science and Technology, Graduate University for financial support.

References:

Aktas T, Avsar Ilik I, Maticzka D, Bhardwaj V, Pessoa Rodrigues C, Mittler G, Manke T, Backofen R, Akhtar A. 2017. Dhx9 suppresses rna processing defects originating from the alu invasion of the human genome. Nature. 544(7648):115-119.

Angeles-Albores D, Lee R, Chan J, Sternberg P. 2018. Two new functions in the wormbase enrichment suite. MicroPubl Biol. 2018.

Angeles-Albores D, RY NL, Chan J, Sternberg PW. 2016. Tissue enrichment analysis for C. elegans genomics. BMC Bioinformatics. 17(1):366.

Ashwal-Fluss R, Meyer M, Pamudurti NR, Ivanov A, Bartok O, Hanan M, Evantal N, Memczak S, Rajewsky N, Kadener S. 2014. Circrna biogenesis competes with pre-mrna splicing. Mol Cell. 56(1):55-66.

Brenner S. 1974. The genetics of caenorhabditis elegans. Genetics. 77(1):71-94.

Buratti E, Baralle FE. 2011. Tdp-43: New aspects of autoregulation mechanisms in rna binding proteins and their connection with human disease. Febs J. 278(19):3530-3538.

Cao D. 2021. Reverse complementary matches simultaneously promote both back-splicing and exon-skipping. BMC Genomics. 22(1):586.

Chen LL. 2020. The expanding regulatory mechanisms and cellular functions of circular rnas. Nat Rev Mol Cell Biol. 21(8):475-490.

Chen W, Schuman E. 2016. Circular rnas in brain and other tissues: A functional enigma. Trends Neurosci. 39(9):597-604.

Cheng J, Metge F, Dieterich C. 2016. Specific identification and quantification of circular rnas from sequencing data. Bioinformatics. 32(7):1094-1096.

Cocquerelle C, Mascrez B, Hetuin D, Bailleul B. 1993. Mis-splicing yields circular rna molecules. Faseb J. 7(1):155-160.

Conn SJ, Pillman KA, Toubia J, Conn VM, Salmanidis M, Phillips CA, Roslan S, Schreiber AW, Gregory PA, Goodall GJ. 2015. The rna binding protein quaking regulates formation of circrnas. Cell. 160(6):1125-1134.

Conn VM, Hugouvieux V, Nayak A, Conos SA, Capovilla G, Cildir G, Jourdain A, Tergaonkar V, Schmid M, Zubieta C et al. 2017. A circrna from sepallata3 regulates splicing of its cognate mrna through r-loop formation. Nat Plants. 3(5):17053.

Damianov A, Black DL. 2010. Autoregulation of fox protein expression to produce dominant negative splicing factors. RNA. 16(2):405-416.

Dichmann DS, Harland RM. 2012. Fus/tls orchestrates splicing of developmental regulators during gastrulation. Genes Dev. 26(12):1351-1363.

Dobin A, Davis CA, Schlesinger F, Drenkow J, Zaleski C, Jha S, Batut P, Chaisson M, Gingeras TR. 2013. Star: Ultrafast universal rna-seq aligner. Bioinformatics. 29(1):15-21.

Dokshin GA, Ghanta KS, Piscopo KM, Mello CC. 2018. Robust genome editing with short single-stranded and long, partially single-stranded DNA donors in caenorhabditis elegans. Genetics. 210(3):781-787.

Du WW, Yang W, Li X, Fang L, Wu N, Li F, Chen Y, He Q, Liu E, Yang Z et al. 2020. The circular rna circska3 binds integrin beta1 to induce invadopodium formation enhancing breast cancer invasion. Mol Ther. 28(5):1287-1298.

Errichelli L, Dini Modigliani S, Laneve P, Colantoni A, Legnini I, Capauto D, Rosa A, De Santis R, Scarfo R, Peruzzi G et al. 2017. Fus affects circular rna expression in murine embryonic stem cell-derived motor neurons. Nat Commun. 8:14741.

Fei T, Chen Y, Xiao T, Li W, Cato L, Zhang P, Cotter MB, Bowden M, Lis RT, Zhao SG et al. 2017. Genome-wide crispr screen identifies hnrnpl as a prostate cancer dependency regulating rna splicing. Proc Natl Acad Sci U S A. 114(26):E5207-E5215.

Gao Y, Zhang J, Zhao F. 2018. Circular rna identification based on multiple seed matching. Brief Bioinform. 19(5):803-810.

Gruner H, Cortes-Lopez M, Cooper DA, Bauer M, Miura P. 2016. Circrna accumulation in the aging mouse brain. Sci Rep. 6:38907.

Hansen TB. 2018. Improved circrna identification by combining prediction algorithms. Front Cell Dev Biol. 6:20.

Hansen TB, Jensen TI, Clausen BH, Bramsen JB, Finsen B, Damgaard CK, Kjems J. 2013. Natural rna circles function as efficient microrna sponges. Nature. 495(7441):384-388.

Hoell JI, Larsson E, Runge S, Nusbaum JD, Duggimpudi S, Farazi TA, Hafner M, Borkhardt A, Sander C, Tuschl T. 2011. Rna targets of wild-type and mutant fet family proteins. Nat Struct Mol Biol. 18(12):1428-1431.

Ishigaki S, Masuda A, Fujioka Y, Iguchi Y, Katsuno M, Shibata A, Urano F, Sobue G, Ohno K. 2012. Position-dependent fus-rna interactions regulate alternative splicing events and transcriptions. Sci Rep. 2:529.

Ivanov A, Memczak S, Wyler E, Torti F, Porath HT, Orejuela MR, Piechotta M, Levanon EY, Landthaler M, Dieterich C et al. 2015. Analysis of intron sequences reveals hallmarks of circular rna biogenesis in animals. Cell Rep. 10(2):170-177.

Jutzi D, Campagne S, Schmidt R, Reber S, Mechtersheimer J, Gypas F, Schweingruber C, Colombo M, von Schroetter C, Loughlin FE et al. 2020. Aberrant interaction of fus with the u1 snrna provides a molecular mechanism of fus induced amyotrophic lateral sclerosis. Nat Commun. 11(1):6341.

Kawamura K, Maruyama IN. 2019. Forward genetic screen for caenorhabditis elegans mutants with a shortened locomotor healthspan. G3 (Bethesda). 9(8):2415-2423.

Kelly S, Greenman C, Cook PR, Papantonis A. 2015. Exon skipping is correlated with exon circularization. J Mol Biol. 427(15):2414-2417.

Khan MA, Reckman YJ, Aufiero S, van den Hoogenhof MM, van der Made I, Beqqali A, Koolbergen DR, Rasmussen TB, van der Velden J, Creemers EE et al. 2016. Rbm20 regulates circular rna production from the titin gene. Circ Res. 119(9):996-1003.

King OD, Gitler AD, Shorter J. 2012. The tip of the iceberg: Rna-binding proteins with prion-like domains in neurodegenerative disease. Brain Res. 1462:61-80.

Kramer MC, Liang D, Tatomer DC, Gold B, March ZM, Cherry S, Wilusz JE. 2015. Combinatorial control of drosophila circular rna expression by intronic repeats, hnrnps, and sr proteins. Genes Dev. 29(20):2168-2182.

Kwiatkowski TJ, Jr., Bosco DA, Leclerc AL, Tamrazian E, Vanderburg CR, Russ C, Davis A, Gilchrist J, Kasarskis EJ, Munsat T et al. 2009. Mutations in the fus/tls gene on chromosome 16 cause familial amyotrophic lateral sclerosis. Science. 323(5918):1205-1208.

Lancaster AK, Nutter-Upham A, Lindquist S, King OD. 2014. Plaac: A web and command-line application to identify proteins with prion-like amino acid composition. Bioinformatics. 30(17):2501-2502.

Li X, Liu CX, Xue W, Zhang Y, Jiang S, Yin QF, Wei J, Yao RW, Yang L, Chen LL. 2017. Coordinated circrna biogenesis and function with nf90/nf110 in viral infection. Mol Cell. 67(2):214-227 e217.

Li Z, Huang C, Bao C, Chen L, Lin M, Wang X, Zhong G, Yu B, Hu W, Dai L et al. 2015. Exon-intron circular rnas regulate transcription in the nucleus. Nat Struct Mol Biol. 22(3):256-264.

Love MI, Huber W, Anders S. 2014. Moderated estimation of fold change and dispersion for rna-seq data with deseq2. Genome Biol. 15(12):550.

Markert SM, Skoruppa M, Yu B, Mulcahy B, Zhen M, Gao S, Sendtner M, Stigloher C. 2019. An als-associated mutation in human fus reduces neurotransmission from C. elegans motor neurons to muscles. bioRxiv.860536.

McGlincy NJ, Tan LY, Paul N, Zavolan M, Lilley KS, Smith CW. 2010. Expression proteomics of upf1 knockdown in hela cells reveals autoregulation of hnrnp a2/b1 mediated by alternative splicing resulting in nonsense-mediated mrna decay. BMC Genomics. 11:565.

Memczak S, Jens M, Elefsinioti A, Torti F, Krueger J, Rybak A, Maier L, Mackowiak SD, Gregersen LH, Munschauer M et al. 2013. Circular rnas are a large class of animal rnas with regulatory potency. Nature. 495(7441):333-338.

Merritt C, Seydoux G. 2010. Transgenic solutions for the germline. WormBook.1-21.

Muller-McNicoll M, Rossbach O, Hui J, Medenbach J. 2019. Auto-regulatory feedback by rna-binding proteins. J Mol Cell Biol. 11(10):930-939.

Murakami T, Qamar S, Lin JQ, Schierle GS, Rees E, Miyashita A, Costa AR, Dodd RB, Chan FT, Michel CH et al. 2015. Als/ftd mutation-induced phase transition of fus liquid droplets and reversible hydrogels into irreversible hydrogels impairs rnp granule function. Neuron. 88(4):678-690.

Murakami T, Yang SP, Xie L, Kawano T, Fu D, Mukai A, Bohm C, Chen F, Robertson J, Suzuki H et al. 2012. Als mutations in fus cause neuronal dysfunction and death in caenorhabditis elegans by a dominant gain-of-function mechanism. Hum Mol Genet. 21(1):1-9.

Nigro JM, Cho KR, Fearon ER, Kern SE, Ruppert JM, Oliner JD, Kinzler KW, Vogelstein B. 1991. Scrambled exons. Cell. 64(3):607-613.

693 Norris AD, Gao S, Norris ML, Ray D, Ramani AK, Fraser AG, Morris Q, Hughes TR, Zhen M,
694 Calarco JA. 2014. A pair of rna-binding proteins controls networks of splicing events
695 contributing to specialization of neural cell types. Mol Cell. 54(6):946-959.
696 Norris AD, Gracida X, Calarco JA. 2017. Crispr-mediated genetic interaction profiling identifies
697 rna binding proteins controlling metazoan fitness. Elife. 6:e28129.
698 Nussbaum-Krammer CI, Neto MF, Brielmann RM, Pedersen JS, Morimoto RI. 2015.
699 Investigating the spreading and toxicity of prion-like proteins using the metazoan model
700 organism c. Elegans. J Vis Exp. (95):52321.
701 Okholm TLH, Sathe S, Park SS, Kamstrup AB, Rasmussen AM, Shankar A, Chua ZM, Fristrup
702 N, Nielsen MM, Vang S et al. 2020. Transcriptome-wide profiles of circular rna and rna-
703 binding protein interactions reveal effects on circular rna biogenesis and cancer pathway
704 expression. Genome Med. 12(1):112.
705 Panda AC, De S, Grammatikakis I, Munk R, Yang X, Piao Y, Dudekula DB, Abdelmohsen K,
706 Gorospe M. 2017. High-purity circular rna isolation method (rpad) reveals vast collection
707 of intronic circrnas. Nucleic Acids Res. 45(12):e116.
708 Rogelj B, Easton LE, Bogu GK, Stanton LW, Rot G, Curk T, Zupan B, Sugimoto Y, Modic M,
709 Haberman N et al. 2012. Widespread binding of fus along nascent rna regulates
710 alternative splicing in the brain. Sci Rep. 2:603.
711 Rossbach O, Hung LH, Schreiner S, Grishina I, Heiner M, Hui J, Bindereif A. 2009. Auto- and
712 cross-regulation of the hnrnp l proteins by alternative splicing. Mol Cell Biol.
713 29(6):1442-1451.
714 Rybak-Wolf A, Stottmeister C, Glazar P, Jens M, Pino N, Giusti S, Hanan M, Behm M, Bartok
715 O, Ashwal-Fluss R et al. 2015. Circular rnas in the mammalian brain are highly abundant,
716 conserved, and dynamically expressed. Mol Cell. 58(5):870-885.
717 Sama RR, Ward CL, Bosco DA. 2014. Functions of fus/tls from DNA repair to stress response:
718 Implications for als. Asn Neuro. 6(4):1-18.
719 Schwartz JC, Ebmeier CC, Podell ER, Heimiller J, Taatjes DJ, Cech TR. 2012. Fus binds the ctd
720 of rna polymerase ii and regulates its phosphorylation at ser2. Genes Dev. 26(24):2690-
721 2695.
722 Stephens M. 2017. False discovery rates: A new deal. Biostatistics. 18(2):275-294.

Sureau A, Gattoni R, Dooghe Y, Stevenin J, Soret J. 2001. Sc35 autoregulates its expression by promoting splicing events that destabilize its mrnas. EMBO J. 20(7):1785-1796.

Tan JH, Fraser AG. 2017. The combinatorial control of alternative splicing in c. Elegans. Plos Genet. 13(11):e1007033.

Therrien M, Rouleau GA, Dion PA, Parker JA. 2016. Fet proteins regulate lifespan and neuronal integrity. Sci Rep. 6:25159.

Thompson M, Bixby R, Dalton R, Vandenburg A, Calarco JA, Norris AD. 2019. Splicing in a single neuron is coordinately controlled by rna binding proteins and transcription factors. Elife. 8.

Vaccaro A, Patten SA, Ciura S, Maios C, Therrien M, Drapeau P, Kabashi E, Parker JA. 2012a. Methylene blue protects against tdp-43 and fus neuronal toxicity in c. Elegans and d. Rerio. Plos One. 7(7):e42117.

Vaccaro A, Tauffenberger A, Aggad D, Rouleau G, Drapeau P, Parker JA. 2012b. Mutant tdp-43 and fus cause age-dependent paralysis and neurodegeneration in c. Elegans. Plos One. 7(2):e31321.

Vance C, Rogelj B, Hortobagyi T, De Vos KJ, Nishimura AL, Sreedharan J, Hu X, Smith B, Ruddy D, Wright P et al. 2009. Mutations in fus, an rna processing protein, cause familial amyotrophic lateral sclerosis type 6. Science. 323(5918):1208-1211.

Veriepe J, Fossouo L, Parker JA. 2015. Neurodegeneration in c. Elegans models of als requires tir-1/sarm1 immune pathway activation in neurons. Nat Commun. 6:7319.

Westholm JO, Miura P, Olson S, Shenker S, Joseph B, Sanfilippo P, Celniker SE, Graveley BR, Lai EC. 2014. Genome-wide analysis of drosophila circular rnas reveals their structural and sequence properties and age-dependent neural accumulation. Cell Rep. 9(5):1966-1980.

Wollerton MC, Gooding C, Wagner EJ, Garcia-Blanco MA, Smith CW. 2004. Autoregulation of polypyrimidine tract binding protein by alternative splicing leading to nonsense-mediated decay. Mol Cell. 13(1):91-100.

Xia P, Wang S, Ye B, Du Y, Li C, Xiong Z, Qu Y, Fan Z. 2018. A circular rna protects dormant hematopoietic stem cells from DNA sensor cgas-mediated exhaustion. Immunity. 48(4):688-701 e687.

You X, Vlatkovic I, Babic A, Will T, Epstein I, Tushev G, Akbalik G, Wang M, Glock C, Quedenau C et al. 2015. Neural circular rnas are derived from synaptic genes and regulated by development and plasticity. Nat Neurosci. 18(4):603-610.

Yu Y, Reed R. 2015. Fus functions in coupling transcription to splicing by mediating an interaction between rnap ii and u1 snrnp. Proc Natl Acad Sci U S A. 112(28):8608-8613.

Zhang T, Wu YC, Mullane P, Ji YJ, Liu H, He L, Arora A, Hwang HY, Alessi AF, Niaki AG et al. 2018. Fus regulates activity of microrna-mediated gene silencing. Mol Cell. 69(5):787-801 e788.

Zhang XO, Dong R, Zhang Y, Zhang JL, Luo Z, Zhang J, Chen LL, Yang L. 2016. Diverse alternative back-splicing and alternative splicing landscape of circular rnas. Genome Res. 26(9):1277-1287.

Zhou Y, Liu S, Liu G, Ozturk A, Hicks GG. 2013. Als-associated fus mutations result in compromised fus alternative splicing and autoregulation. Plos Genet. 9(10):e1003895.

Zhu YJ, Zheng B, Luo GJ, Ma XK, Lu XY, Lin XM, Yang S, Zhao Q, Wu T, Li ZX et al. 2019. Circular rnas negatively regulate cancer stem cells by physically binding fmrp against ccar1 complex in hepatocellular carcinoma. Theranostics. 9(12):3526-3540.

Figure Legends

Figure 1. RBP screening identifies FUST-1 as a circRNA regulator

(A) Heatplot showing the fold changes of circRNAs in 13 RBP mutant strains compared with wild-type N2 strain at the L1 stage. Foldchanges are quantified by RT-qPCR and normalized to the N2 strain using *pmp-3* as the reference gene. Blue color means downregulation and red color means upregulation.

(B) Illustration of primer strategy of circRNA detection. Note the positions of divergent primers to amplify the back-spliced junction (BSJ) sequences.

(C) Gene structure of *fust-1* in wild-type N2 strain and the two mutant strains.

(D) RT-qPCR quantification of circRNA levels in wild-type N2 strain and *fust-1(tm4439)* strain. Levels are normalized to the N2 strain using *pmp-3* as the reference gene. Results are shown as mean ± sd of three biological replicates. Two-tailed Student's *t*-test. $p<0.05$, $^{**}p < 0.01$, $^{***}p < 0.001$.

(E) Representative images showing the expression pattern of mRFP-fused FUST-1 in *fust-1(csb21)* strain. Note the pharyngeal GFP expression in *fust-1(csb21)*. Scale bars: 50 μm.

(F) RT-qPCR quantification of circRNAs in the indicated strains. Levels are normalized to the N2 strain using *pmp-3* as the reference gene. Results are shown as mean ± sd of three biological replicates. One-way ANOVA, Tukey's multiple comparisons. $^{*}p<0.05$, $^{**}p < 0.01$, $^{***}p < 0.001$, $^{****}p < 0.0001$; ns, not significant.

Figure 2. FUST-1 regulates circRNAs without affecting the cognate linear mRNAs

(A) Illustration of primer positions used to distinguish full-length mRNA and circRNA from the same gene.

(B) RT-qPCR quantification of circRNAs and their linear mRNAs in the N2 strain and *fust-1(csb21)* strain at the L1 stage. Levels are normalized to the N2 strain using *pmp-3* as the reference gene. Results are shown as mean ± sd of three biological replicates. Two-tailed Student's *t*-test. ***$p < 0.001$, ****$p < 0.0001$; ns, not significant.

(C) Gene structure of *zip-2* and the positions of probes used for northern blot. Probe 1 can detect both full-length *zip-2* mRNA and *circ-zip-2*. Probe 2 spans the BSJ, which is specific *to circ-zip-2*. The lengths of the two probes are labeled.

(D) Northern blot detection of *zip-2* transcripts (probe1) and *act-1* mRNA at the L1 stage of N2 strain and *fust-1(csb21)* strain. The theoretical lengths of each transcript are labeled. Results are from three biological replicates.

(E) Quantification of northern blot results in (D), normalized to N2 strain using *act-1* as the reference gene. Gel regions used for quantification are shown in Figure S3B. Results are shown as mean ± sd. Two-tailed Student's *t*-test. **$p < 0.01$, ***$p < 0.001$.

(F) Steps involved in library preparation of RNA-seq using rRNA-depletion (ribo$^-$ only) and the RPAD method.

(G) Representative coverages of RNA-seq results of *zip-2*. The BSJ reads of *circ-zip-2* in each group are shown. Scales of the ribo$^-$ group and the RPAD group are 0-1800.and 0-10000, respectively. Note the depletion of reads in the non-circRNA-producing exons of *zip-2* (red rectangles) and the increase of BSJ reads in the RPAD group (numbers in the arcs).

(H) Scatter plot showing the log2 fold changes of 4956 circRNAs (RPAD) versus log2 fold changes of their corresponding linear mRNAs (ribo$^-$). circRNAs or mRNAs that show > 1.5-fold changes with adjusted *p* value < 0.05 are considered significantly altered. The Pearson correlation coefficient (*R*) and *p* value (*p*) are shown. Names of several circRNA genes are labeled.

(I) Scatter plot showing the log2 fold changes of 910 overlapped circRNAs between the "N2-*fust-1(csb21)"* dataset and the "sort-whole" dataset. circRNAs that show > 1.5-fold changes with adjusted *p* value < 0.05 are considered significantly altered. Names of several circRNA genes are labeled. The Pearson correlation coefficient (*R*) and *p* value (*p*) are shown.

Figure 3. FUST-1 binds to pre-mRNAs of circRNA genes

(A) Sequence confirmation for N-terminal fusion of a FLAG tag just after the start codon of FUST-1. Note the position of gRNA and the mutated PAM site (AGG>AGC).

(B) Western blot showing the co-immunoprecipitation (Co-IP) of FLAG::FUST-1.

(C) Ct value changes of pre-mRNAs of some circRNA genes and rRNAs before and after Co-IP of FLAG::FUST-1 with or without anti-FLAG antibody. Results from 3 biological replicates are shown. Paired two-tailed Student's *t*-test. *$p < 0.05$, **$p < 0.01$, ns, not significant.

Figure 4. FUST-1 regulates both exon-skipping and back-splicing.

(A) Illustration of a gene producing three transcripts: a full-length mRNA, a circRNA, and a skipped transcript that skips the circRNA-producing exon. Positions of primers to specifically detect each transcript are shown.

(B) Sashimi plot showing numbers of reads aligned to the canonical splice junction, the skipped junction, and the back-splice junction in *zip-2*. The coverage data are from the ribo$^-$ dataset. Exons in the red rectangle are circularized.

(C, D) RT-qPCR quantification of levels of the circular, skipped, and full-length linear transcripts in *zip-2* (C) and *arl-13* (D) between wild-type N2 strain and *fust-1(csb21)* strain. Levels are normalized to the N2 strain using *pmp-3* as the reference gene. Results are shown as mean ± sd of three biological replicates. Two-tailed Student's *t*-test. *$p < 0.05$, **$p < 0.01$, *** $p < 0.001$, ns, not significant.

Figure 5. An autoregulation loop in *fust-1*.

(A) Gene structure of *fust-1* and the domains in FUST-1A and FUST-1B. The alternatively spliced exon 5 is outlined in red, which is missing in the cDNA of FUST-1B. Dashed lines link the coding exons to the protein regions in each isoform. Note the positions where nonsense mutations were introduced. Lengths of amino acids in each isoform were labeled. RRM: RNA recognition motif; ZnF: Zinc-figure; NLS: nuclear localization signal.

(B, C) Confocal images showing expression of FUST-1A and FUST-1B in the nucleus of neuron cells (B) and eggs (C). Note that in early eggs, FUST-1A was expressed earlier than FUST-1B (white arrows). Worm stage: day 1 adult. A: Anterior, D: Dorsal. Scale bars: 50 μm.

(D) Representative confocal images showing the expression patterns of splicing reporter of *fust-1* exon 5 in the N2 strain and the *fust-1(csb21)* strain. Worm stage: day 1 adult. Inset squares show the enlarged neck neurons in indicated strains. A: Anterior, D: Dorsal. Scale bars: 50 μm.

(E, F) Quantification of mCherry-to-GFP ratios of the *fust-1* exon5 splicing reporter in the indicated strains. One-way ANOVA, Tukey's multiple comparisons. $^{**}p < 0.01$, $^{***}p < 0.001$, $^{****}p < 0.0001$; ns, not significant.

(G) Ct value changes of *fust-1* pre-mRNA before and after Co-IP of FLAG::FUST-1 with or without anti-FLAG antibody. Primer positions are in intron 4 of *fust-1* pre-mRNA. Results from 3 biological replicates are shown. Paired two-tailed Student's *t*-test. $^{**}p < 0.01$.

Figure 6. FUST-1A is the functional isoform in circRNA regulation

(A) Rescue of circRNA levels by FUST-1 isoforms, quantified by RT-qPCR. cDNA samples from L1 worms of indicated strains were used.

(B) RT-qPCR quantification of circRNA levels at the L1 stage of indicated strains. (A, B) Levels are normalized to N2 strain using *pmp-3* as the reference gene. Results are shown as mean ± sd of three biological replicates. One-way ANOVA, Tukey's multiple comparisons. $^{*}p < 0.05$, $^{**}p < 0.01$, $^{***}p < 0.001$, $^{****}p < 0.0001$; ns, not significant.

(C, D) Prion-like domain prediction results of FUST-1A (C) and FUST-1B (D) from the PLAAC algorithm. A higher PrD.like score (red line) suggests a higher probability of being a PrLD. Note the difference between the N-termini of the two isoforms (dashed rectangles).

Figure 7. A summary model for the autoregulation loop in *fust-1*.

The full-length mRNA of *fust-1* produces FUST-1A, which binds to its own pre-mRNA to promote the skipping of exon 5, resulting in the production of FUST-1B. FUST-1A is the functional isoform in circRNA regulation. While FUST-1B has the same functional domains, it cannot regulate either back-splicing or the exon-skipping of *fust-1* pre-mRNA.

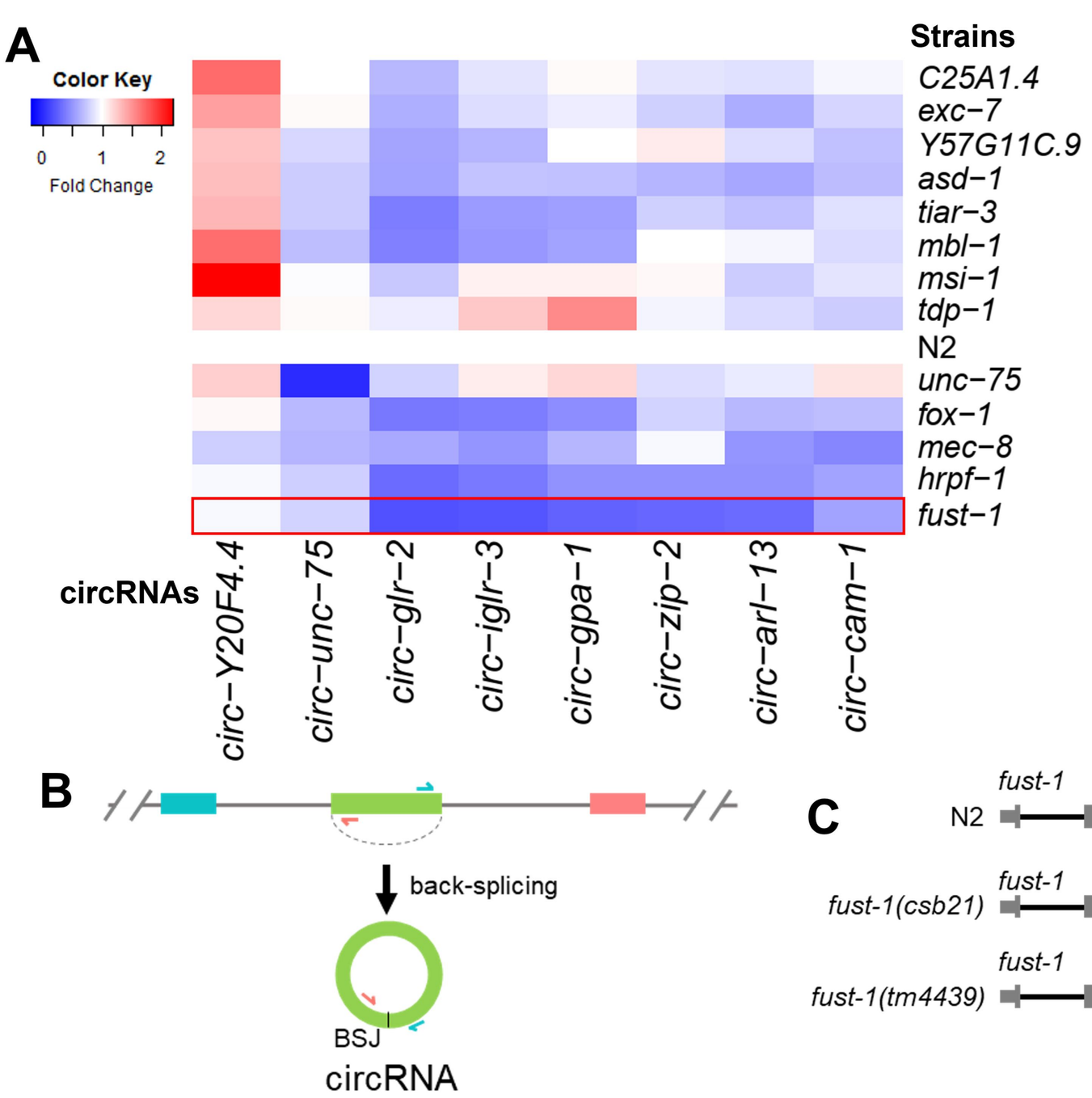
A
Color Key
0
1
2
Fold Change
Strains
C25A1.4
exc−7
Y57G11C.9
asd−1
tiar−3
mbl−1
msi−1
tdp−1
N2
unc−75
fox−1
mec−8
hrpf−1
fust−1
circRNAs
circ−Y20F4.4
circ−unc−75
circ−glr−2
circ−iglr−3
circ−gpa−1
circ−zip−2
circ−arl−13
circ−cam−1

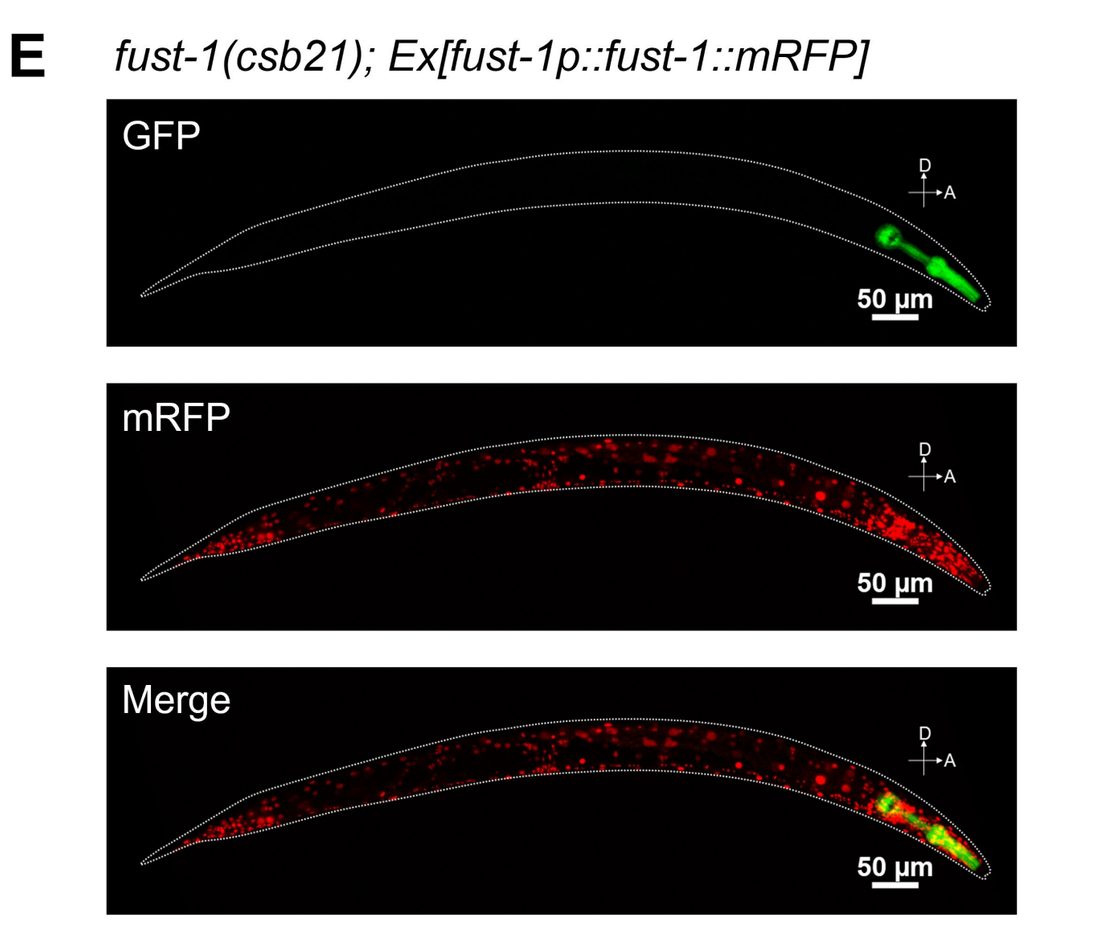
E
fust-1(csb21); Ex[fust-1p::fust-1::mRFP]
GFP
mRFP
Merge
D
A
50 μm

B
back-splicing
BSJ
circRNA

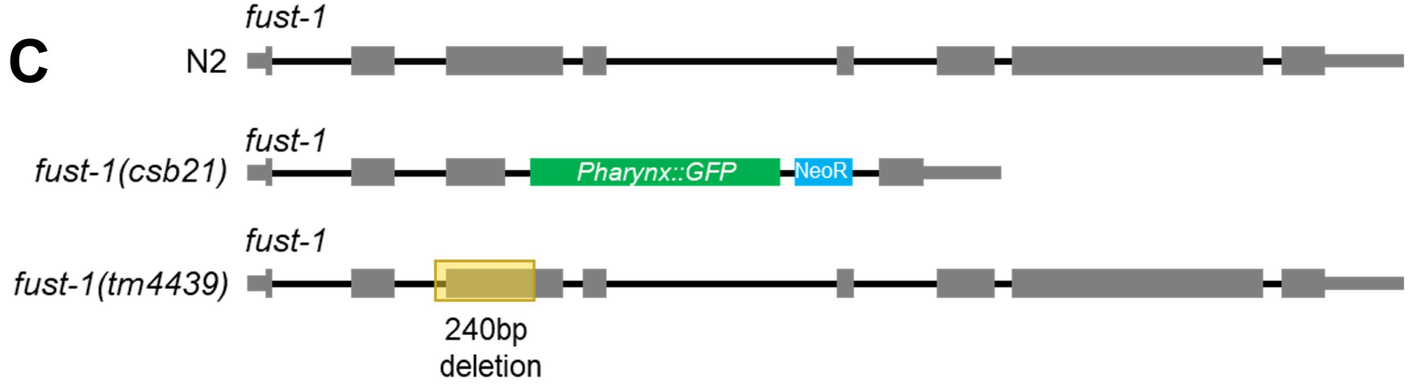
C
fust-1
N2
fust-1
fust-1(csb21)
Pharynx::GFP
NeoR
fust-1
fust-1(tm4439)
240bp
deletion

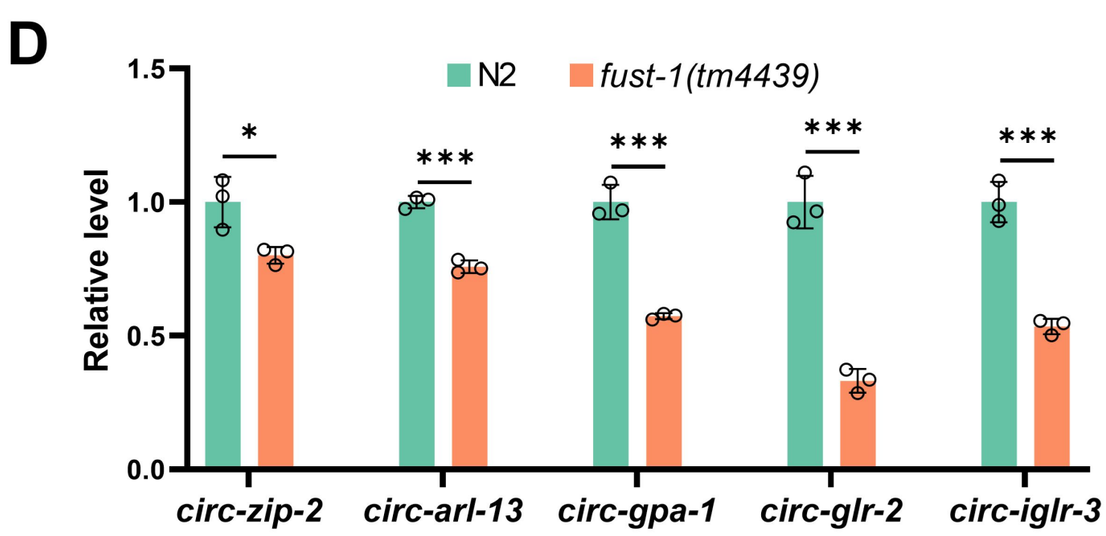
D
N2
fust-1(tm4439)
Relative level
1.5
1.0
0.5
0.0
circ-zip-2
circ-arl-13
circ-gpa-1
circ-glr-2
circ-iglr-3

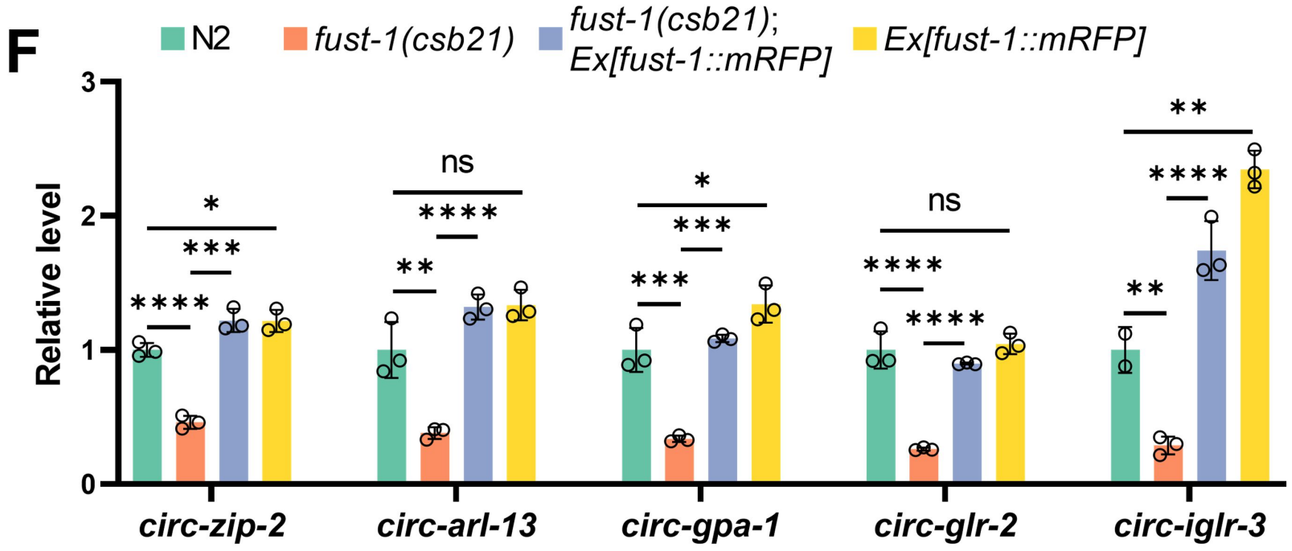
F
N2
fust-1(csb21)
fust-1(csb21); Ex[fust-1::mRFP]
Ex[fust-1::mRFP]
Relative level
3
2
1
0
circ-zip-2
circ-arl-13
circ-gpa-1
circ-glr-2
circ-iglr-3

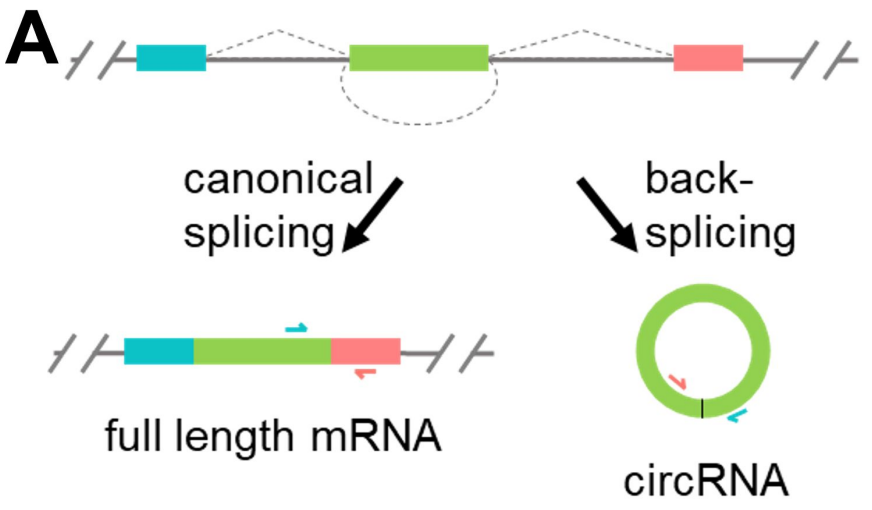
A
canonical splicing
back-splicing
full length mRNA
circRNA

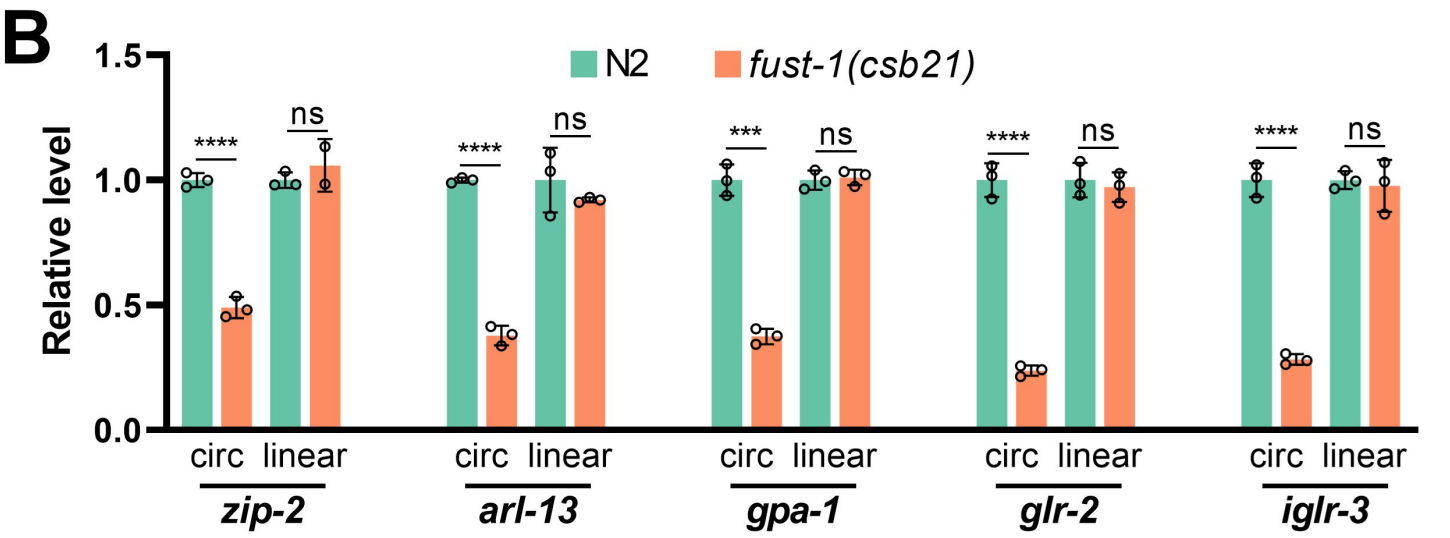
B
N2
fust-1(csb21)
Relative level
1.5
1.0
0.5
0.0
****
ns
***
circ linear
zip-2
arl-13
gpa-1
glr-2
iglr-3

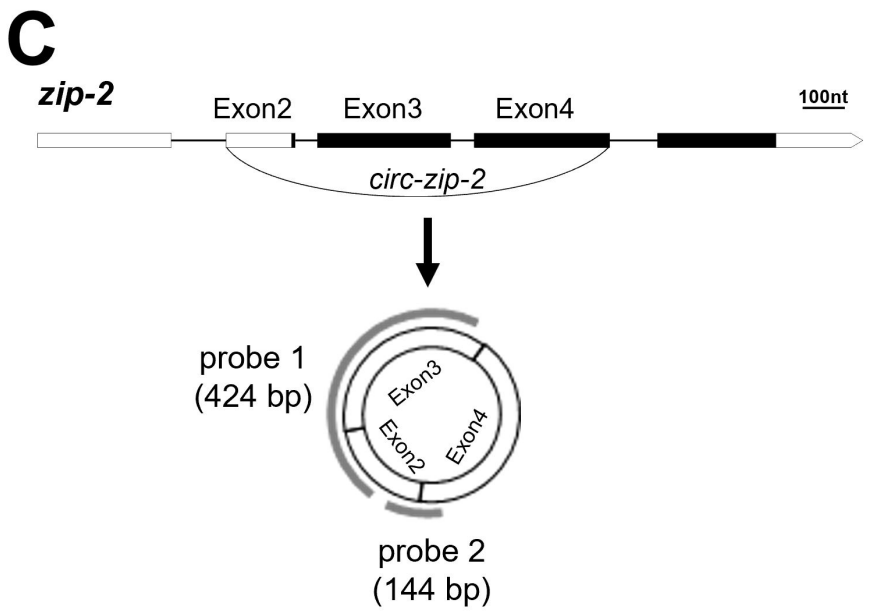
C
zip-2
Exon2
Exon3
Exon4
100nt
circ-zip-2
probe 1
(424 bp)
probe 2
(144 bp)

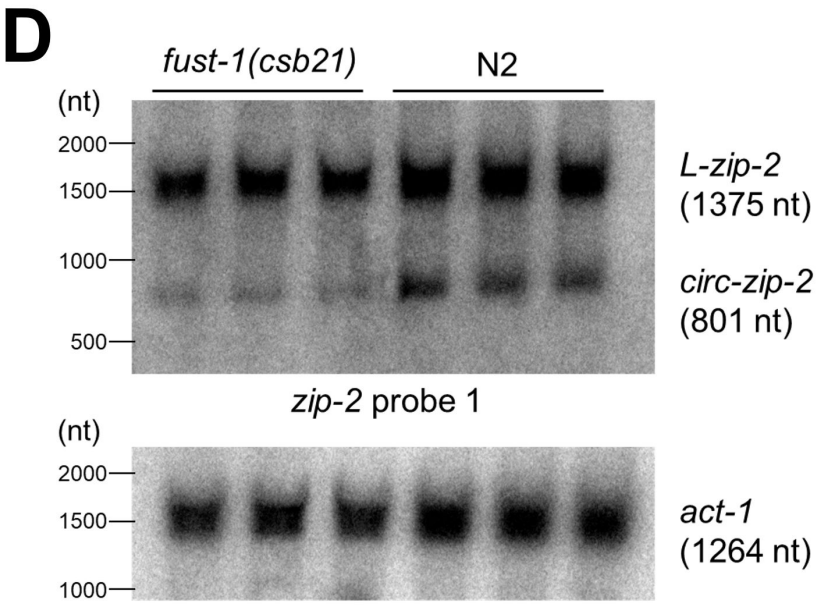
D
fust-1(csb21)
N2
(nt)
2000
1500
1000
500
L-zip-2
(1375 nt)
circ-zip-2
(801 nt)
zip-2 probe 1
act-1
(1264 nt)

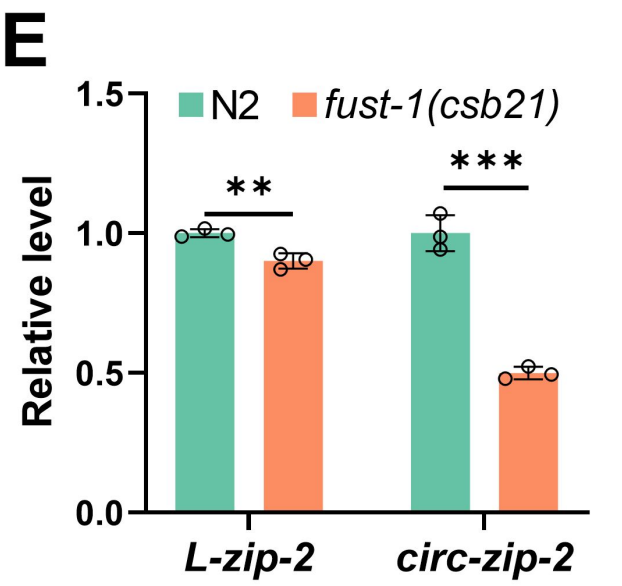
E
N2
fust-1(csb21)
Relative level
1.5
1.0
0.5
0.0
**
***
L-zip-2
circ-zip-2

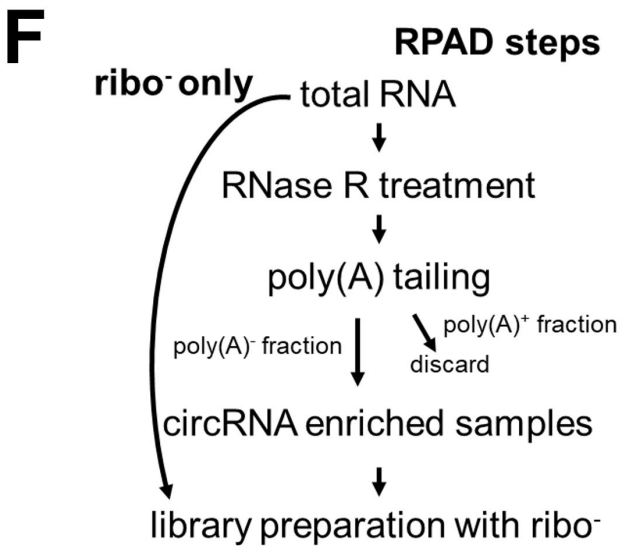
F
RPAD steps
ribo- only
total RNA
RNase R treatment
poly(A) tailing
poly(A)- fraction
poly(A)+ fraction
discard
circRNA enriched samples
library preparation with ribo-

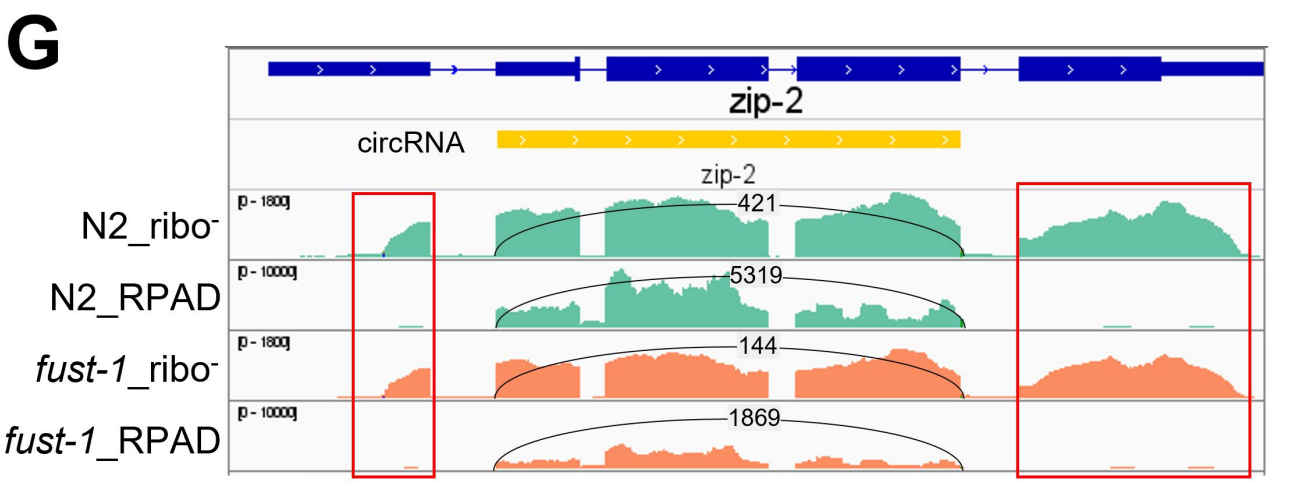
G
zip-2
circRNA
zip-2
N2_ribo-
N2_RPAD
fust-1_ribo-
fust-1_RPAD
421
5319
144
1869

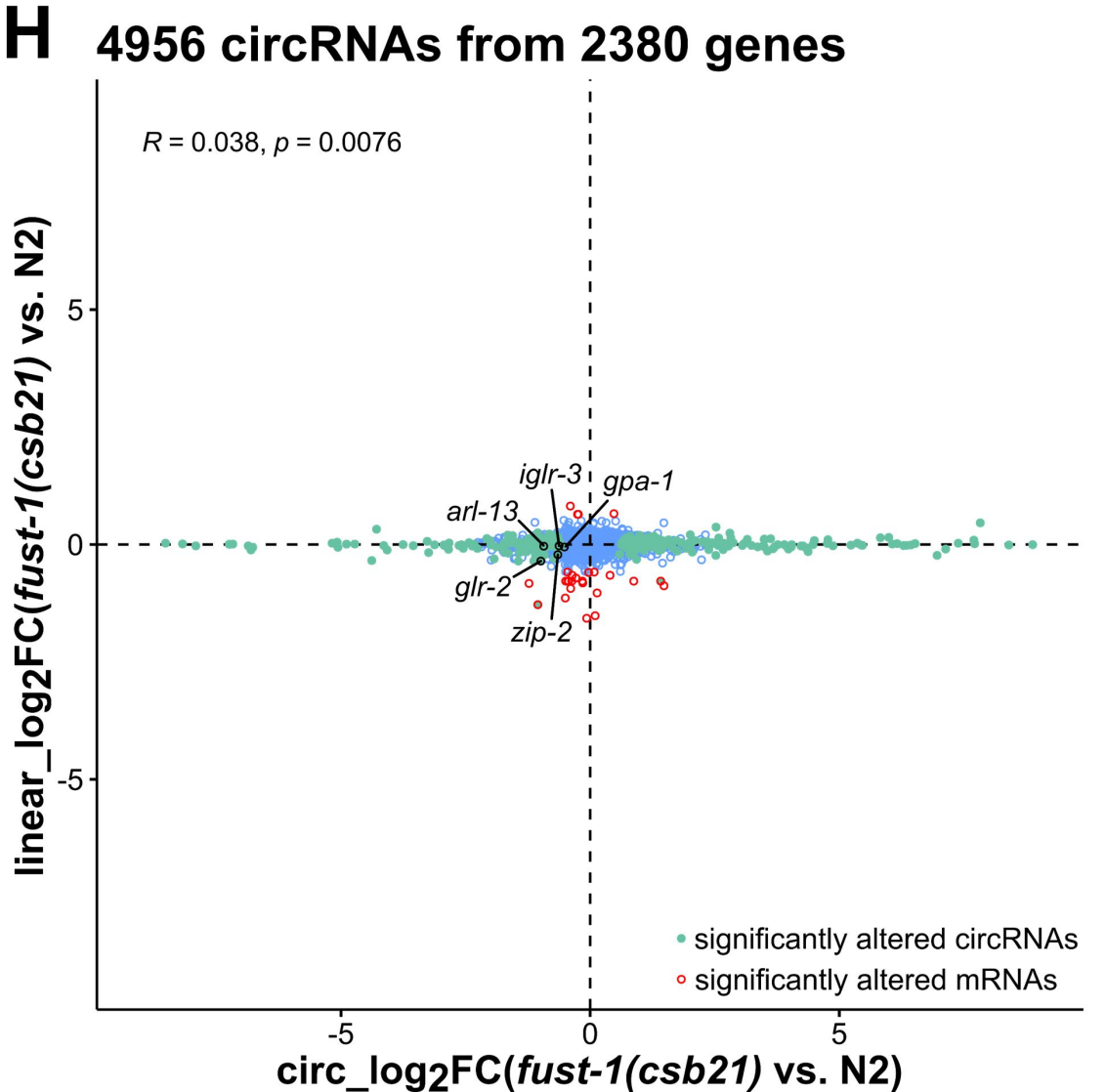
H
4956 circRNAs from 2380 genes
R = 0.038, p = 0.0076
linear_log2FC(fust-1(csb21) vs. N2)
circ_log2FC(fust-1(csb21) vs. N2)
iglr-3
gpa-1
arl-13
glr-2
zip-2
significantly altered circRNAs
significantly altered mRNAs

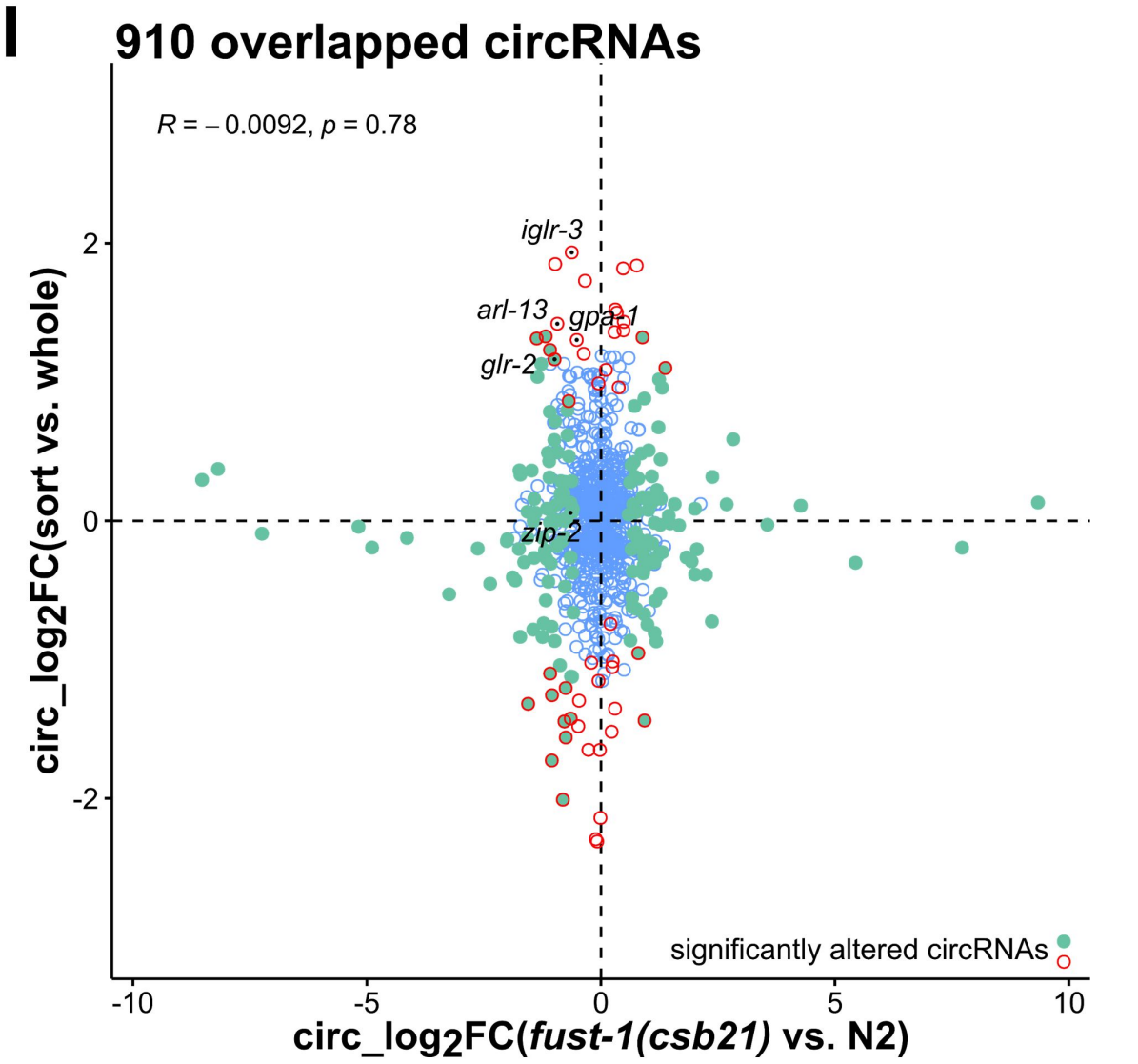
I
910 overlapped circRNAs
R = – 0.0092, p = 0.78
circ_log2FC(sort vs. whole)
circ_log2FC(fust-1(csb21) vs. N2)
iglr-3
arl-13
gpa-1
glr-2
zip-2
significantly altered circRNAs

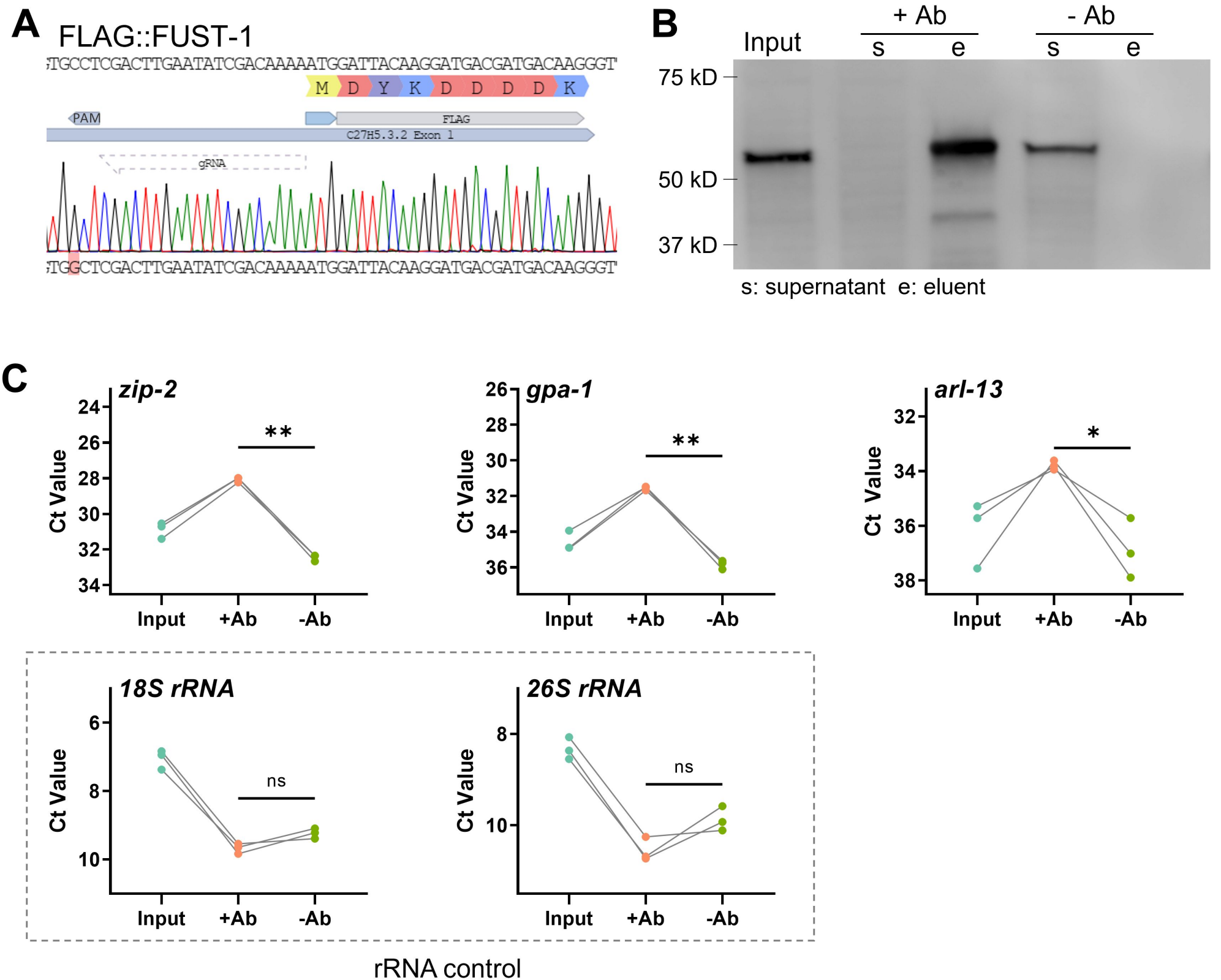
A
FLAG::FUST-1
TGCCTCGACTTGAATATCGACAAAAATGGATTACAAGGATGACGATGACAAGGGT
M D Y K D D D D K
PAM
FLAG
C27H5.3.2 Exon 1
gRNA
TGGCTCGACTTGAATATCGACAAAAATGGATTACAAGGATGACGATGACAAGGGT
B
Input
+ Ab
- Ab
s
e
s
e
75 kD
50 kD
37 kD
s: supernatant e: eluent
C
zip-2
gpa-1
arl-13
18S rRNA
26S rRNA
Ct Value
**
**
*
ns
ns
Input
+Ab
-Ab
rRNA control

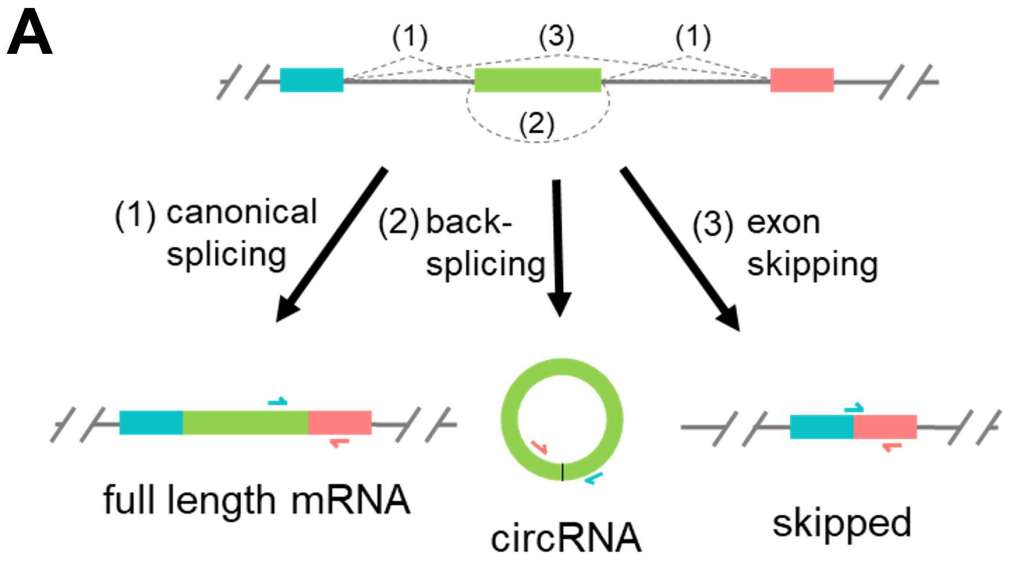
A
(1)
(3)
(1)
(2)
(1) canonical splicing
(2) back-splicing
(3) exon skipping
full length mRNA
circRNA
skipped

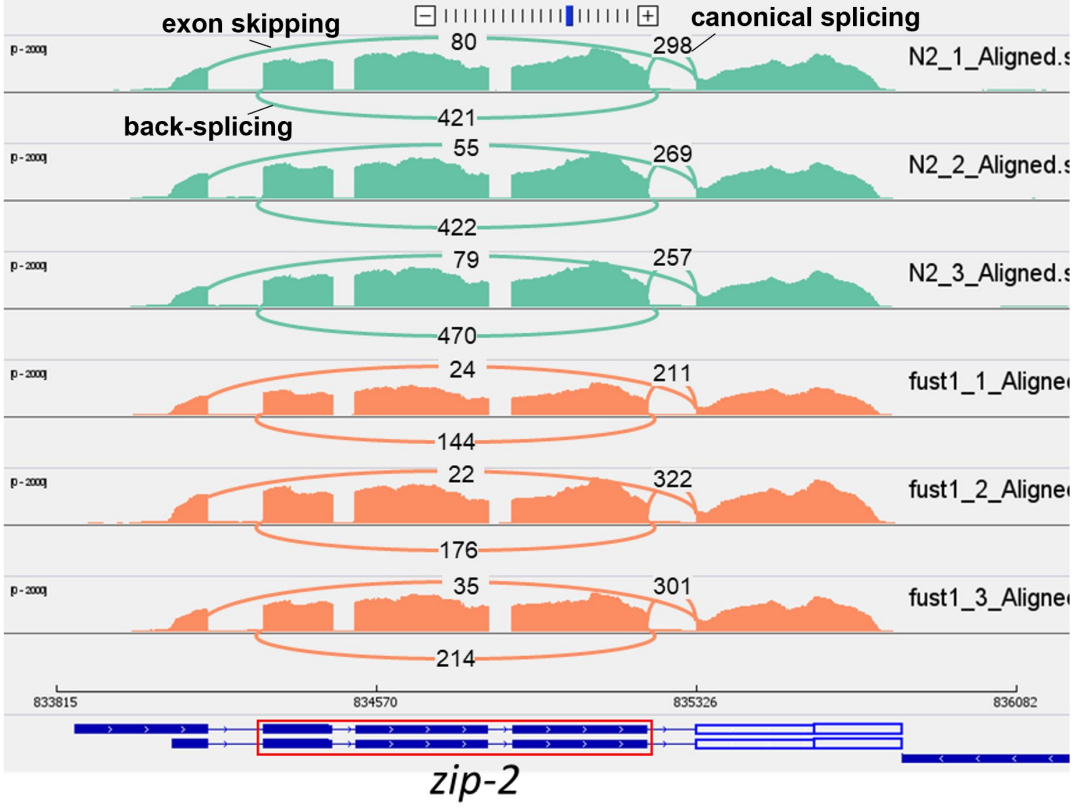
B
exon skipping
canonical splicing
back-splicing
80
298
421
55
269
422
79
257
470
24
211
144
22
322
176
35
301
214
N2_1_Aligned.s
N2_2_Aligned.s
N2_3_Aligned.s
fust1_1_Aligne
fust1_2_Aligne
fust1_3_Aligne
833815
834570
835326
836082
zip-2

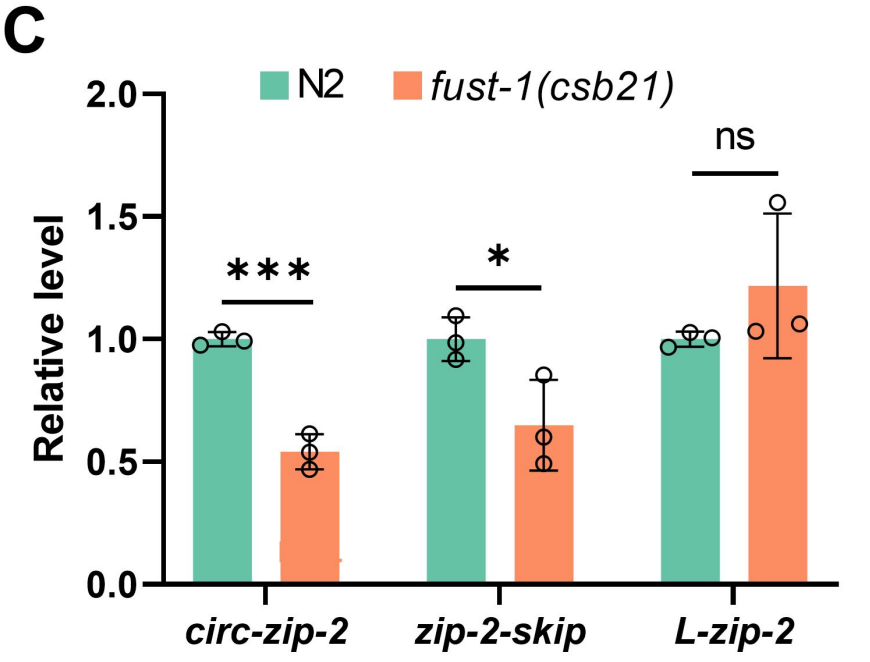
C
N2
fust-1(csb21)
Relative level
2.0
1.5
1.0
0.5
0.0
***
*
ns
circ-zip-2
zip-2-skip
L-zip-2

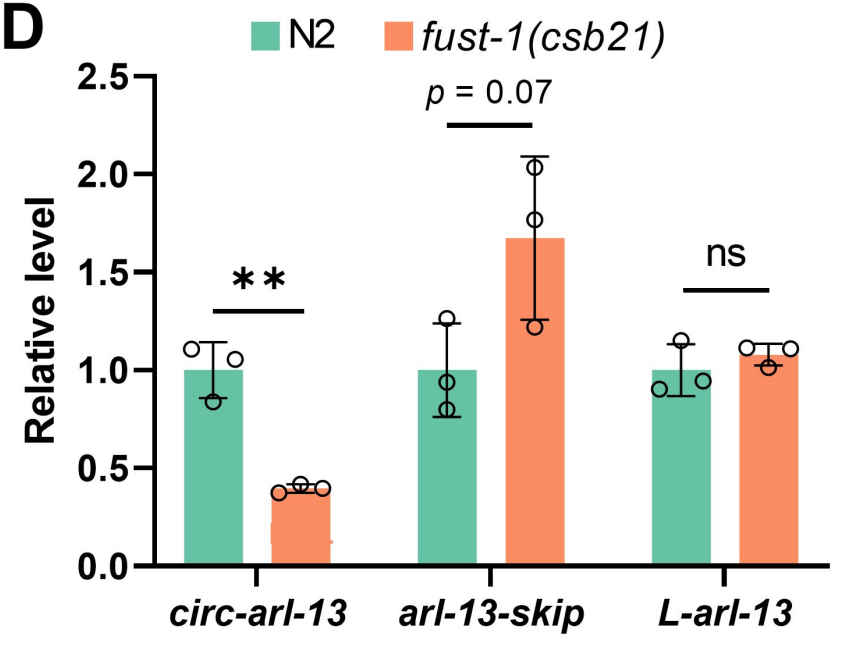
D
N2
fust-1(csb21)
p = 0.07
Relative level
2.5
2.0
1.5
1.0
0.5
0.0
**
ns
circ-arl-13
arl-13-skip
L-arl-13

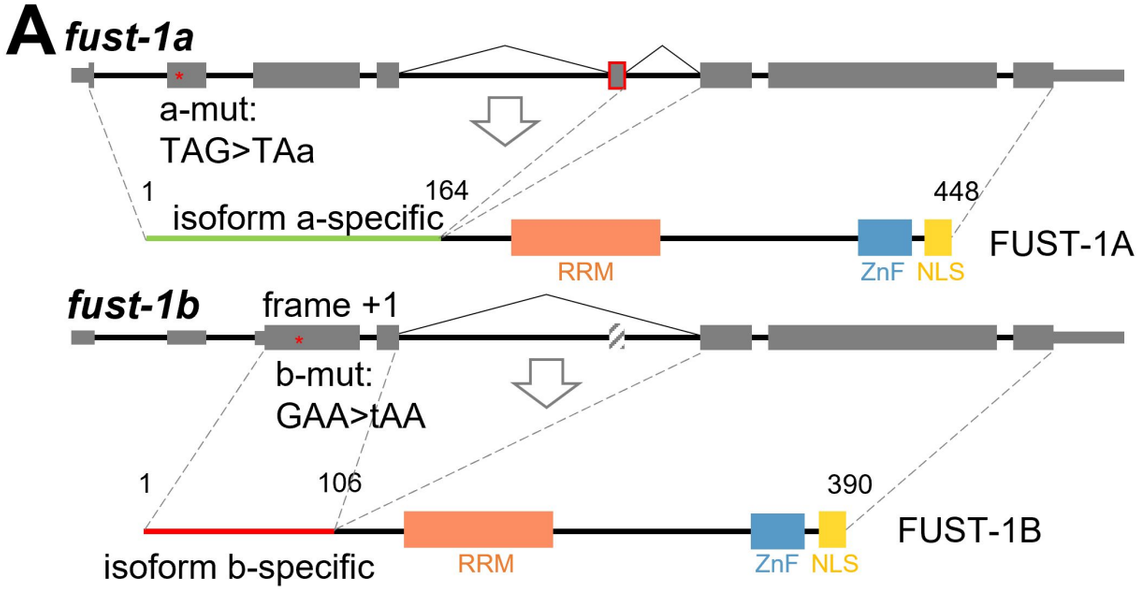

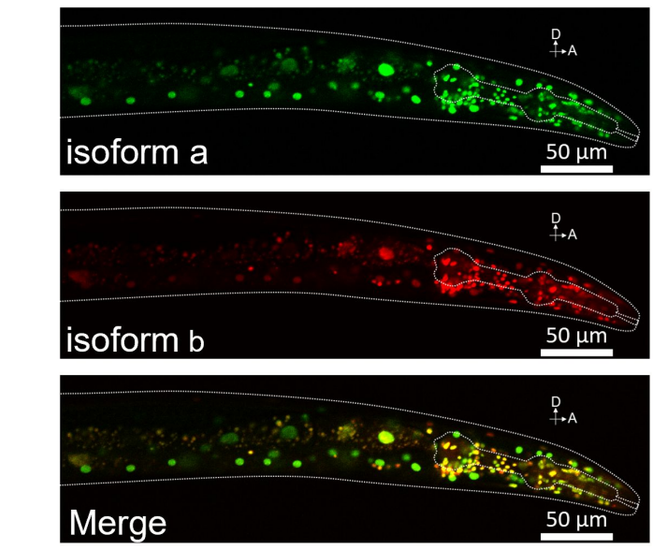

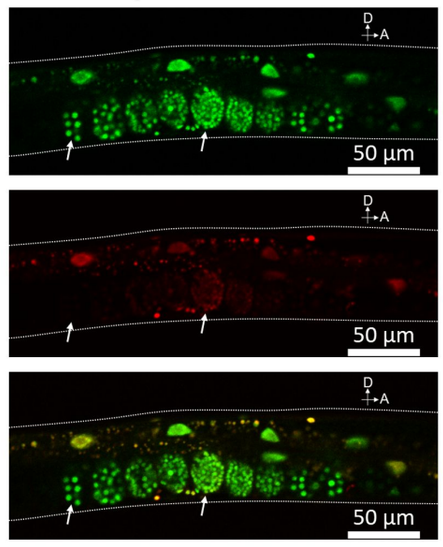

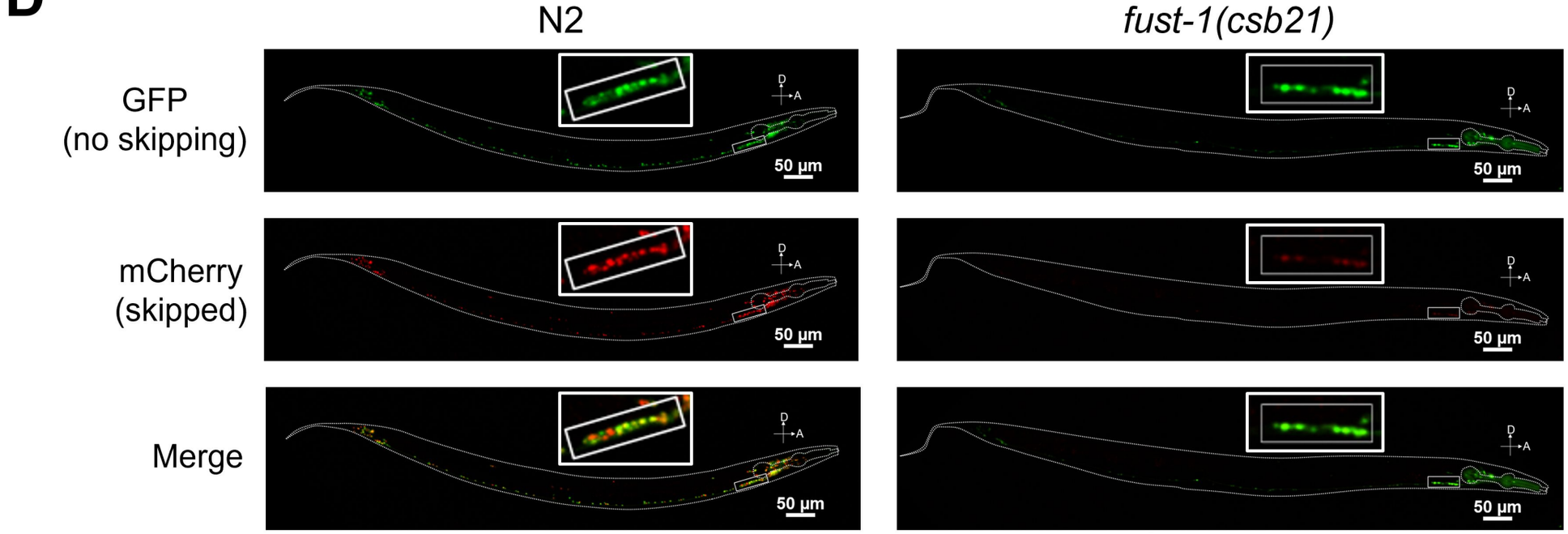

fust-1 exon 5 splicing reporter
Ex[rgef-1p::fust-1(E4-6)::GFP::mCherry::unc-54 3'UTR]

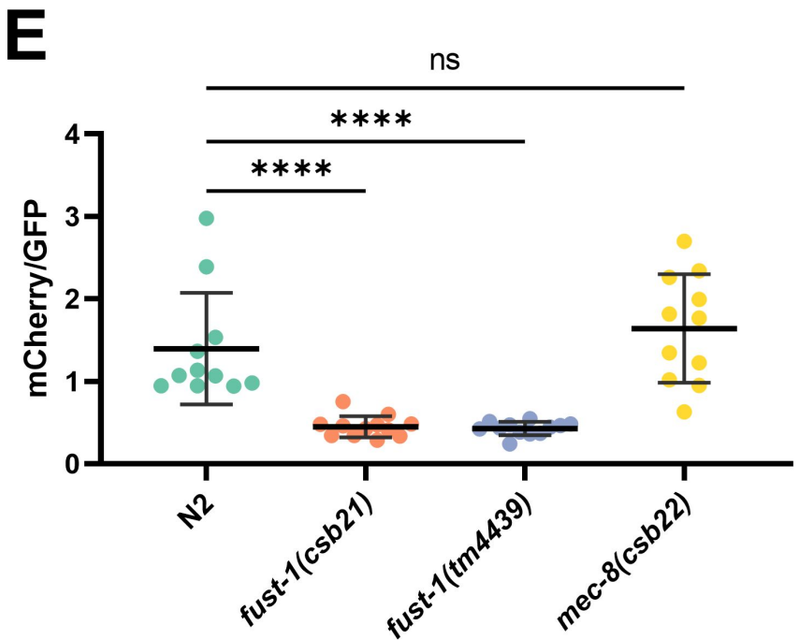

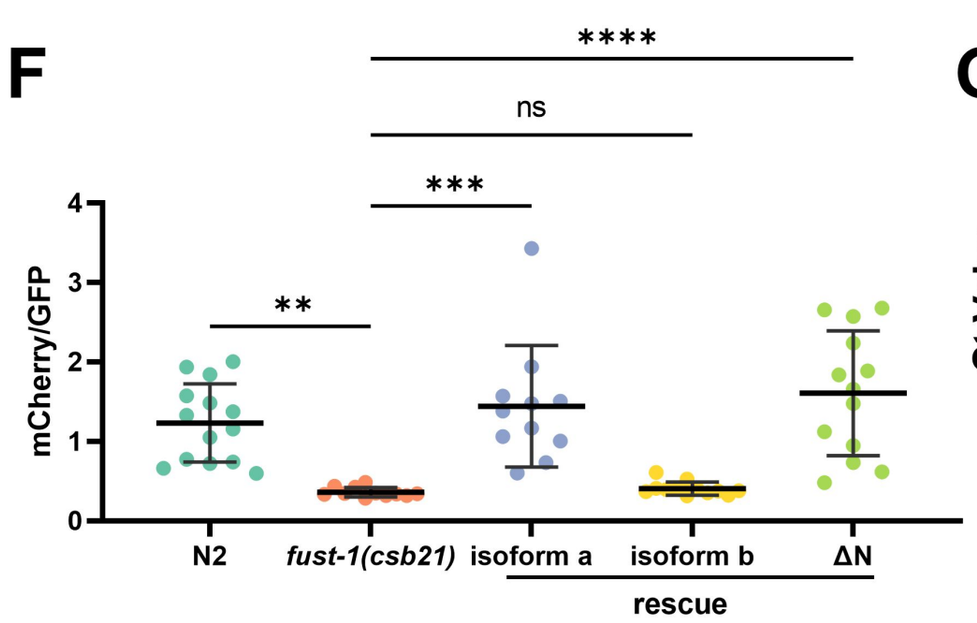

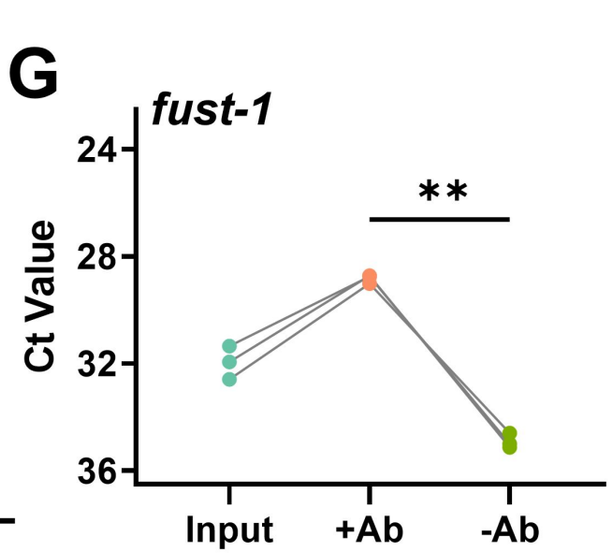

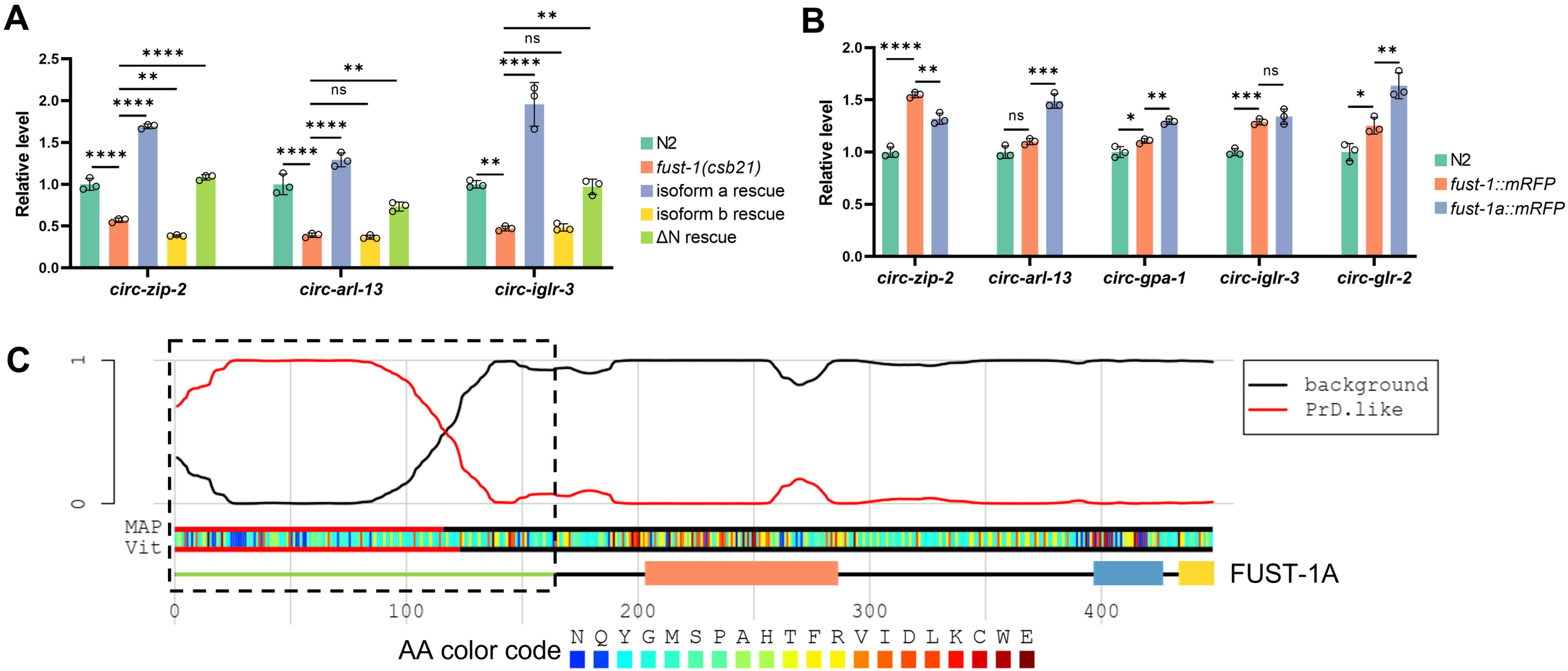
A
Relative level
circ-zip-2
circ-arl-13
circ-iglr-3
N2
fust-1(csb21)
isoform a rescue
isoform b rescue
ΔN rescue
B
Relative level
circ-zip-2
circ-arl-13
circ-gpa-1
circ-iglr-3
circ-glr-2
N2
fust-1::mRFP
fust-1a::mRFP
C
background
PrD.like
MAP
Vit
FUST-1A
AA color code
N Q Y G M S P A H T F R V I D L K C W E
D
background
PrD.like
MAP
Vit
FUST-1B

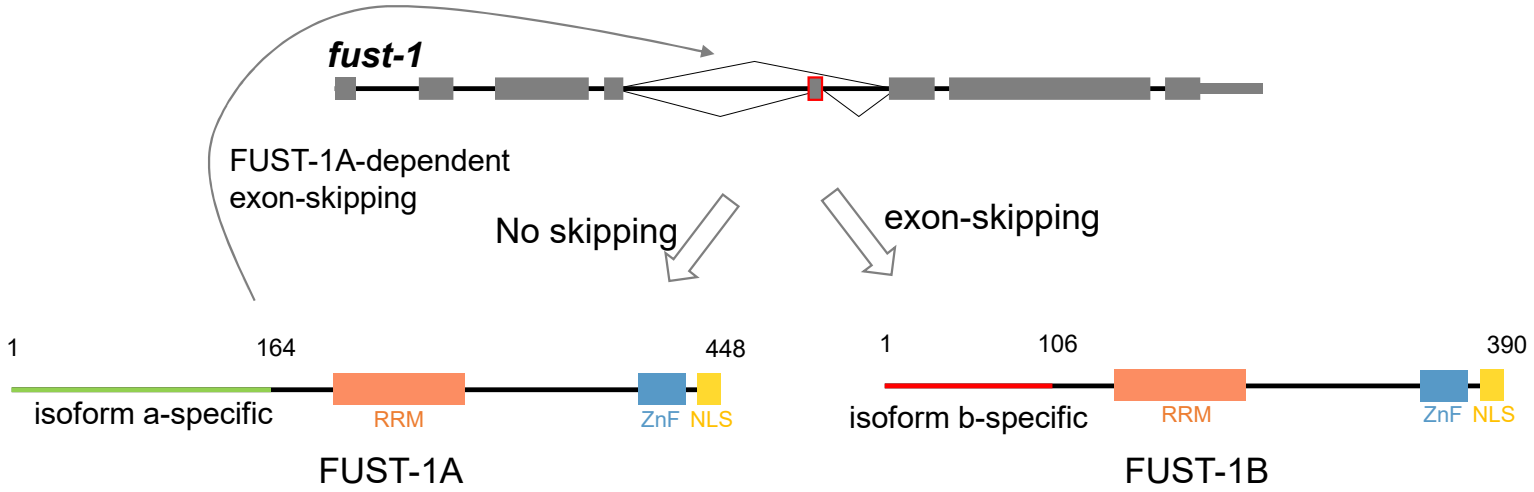

- circRNA regulation ✓
- autoregulation ✓

- circRNA regulation ×
- autoregulation ×